Biosensors and Bioelectronics 89 (2017) 167–186

Contents lists available at ScienceDirect

Biosensors and Bioelectronics

journal homepage: www.elsevier.com/locate/bios

Electrochemical sensors and biosensors based on less aggregated graphene

Xiangjie Bo, Ming Zhou *, Liping Guo *

Key Laboratory of Nanobiosensing and Nanobioanalysis at Universities of Jilin Province, Department of Chemistry, Northeast Normal University, 5268 Renmin Street, Changchun, Jilin Province 130024, PR China

ARTICLE INFO

Article history:
Received 26 April 2016
Accepted 2 May 2016
Available online 3 May 2016

Keywords:
Electrochemical sensors and biosensors
Less aggregated graphene
Porous graphene
Structural engineering
Surface-functionalized graphene

ABSTRACT

As a novel single-atom-thick sheet of sp^2 hybridized carbon atoms, graphene (GR) has attracted extensive attention in recent years because of its unique and remarkable properties, such as excellent electrical conductivity, large theoretical specific surface area, and strong mechanical strength. However, due to the π-π interaction, GR sheets are inclined to stack together, which may seriously degrade the performance of GR with the unique single-atom layer. In recent years, an increasing number of GR-based electrochemical sensors and biosensors are reported, which may reflect that GR has been considered as a kind of hot and promising electrode material for electrochemical sensor and biosensor construction. However, the active sites on GR surface induced by the irreversible GR aggregations would be deeply secluded inside the stacked GR sheets and therefore are not available for the electrocatalysis. So the alleviation or the minimization of the aggregation level for GR sheets would facilitate the exposure of active sites on GR and effectively upgrade the performance of GR-based electrochemical sensors and biosensors. Less aggregated GR with low aggregation and high dispersed structure can be used in improving the electrochemical activity of GR-based electrochemical sensors or biosensors. In this review, we summarize recent advances and new progress for the development of electrochemical sensors based on less aggregated GR. To achieve such goal, many strategies (such as the intercalation of carbon materials, surface modification, and structural engineering) have been applied to alleviate the aggregation level of GR in order to enhance the performance of GR-based electrochemical sensors and biosensors. Finally, the challenges associated with less aggregated GR-based electrochemical sensors and biosensors as well as related future research directions are discussed.

Contents

Abbreviations: APAP, acetaminophen; AA, ascorbic acid; AFM, atomic force microscopy; CNTs, carbon nanotubes; CEA, carcinoembryonic antigen; CVD, chemical vapor deposition; Chox, cholesterol oxidase; Co3O4, cobalt oxide; CV, cyclic voltammogram; CD, cyclodextrin; DA, dopamine; ERGO, electrochemically reduced GO; ECL, electrochemiluminescence; ET, electron-transfer; FET, field-effect transistor; GC, glassy carbon; Gox, glucose oxidase; GONW, GO nanowall; GR, grapheme; GO, graphene oxide; HRP, horseradish peroxidase; H_2O_2, hydrogen peroxide; HP-β-CD, hydroxypropyl-β-CD; IL, ionic liquid; LBL, layer-by-layer; LOD, limit of detection; LUMO, lowest unoccupied molecular orbital; HOMO, highest occupied molecular orbital; MG, methylene green; MIP, molecularly imprinted polymer; NPs, nanoparticles; NWA, nanowire arrays; NADH, nicotinamide adenine dinucleotide; NO, nitric oxide; PTCA, perylene tetracarboxylic acid; POM, polyoxometalate; PDDA, poly (diallyldimethylammonium chloride); PAA, poly(acrylic acid); PSS, poly(styrene sulfonate); PQ11, poly[(2-ethyldimethylammonioethyl methacrylate ethyl sulfate)-*co*-(1-vinylpyrrolidone)]; PFIL, polyethylenimine-functionalized IL; PVP, polyvinylpyrrolidone; QDs, quantum dots; RGNW, reduced GR nanowall; RGNS, reduced GR nanosheet; SEM, scanning electron microscope; SDBS, sodium dodecyl benzene sulfonate; (*s*-GR), sulfonic acid functionalized GR; TEM, transmission electron microscopy; 2D, two-dimensional; UA, uric acid; VACNTs, vertically aligned CNTs

* Corresponding authors.
E-mail addresses: zhoum739@nenu.edu.cn (M. Zhou), guolp078@nenu.edu.cn (L. Guo).

http://dx.doi.org/10.1016/j.bios.2016.05.002
0956-5663/

1. Introduction

Two-dimensional (2D) materials with atomic thickness are considered as a kind of ideal building blocks for the design of various novel functional materials because of their novel electronic, optical, and mechanical properties (Guo et al., 2015). The atomically thick 2D materials not only inherit the properties from their corresponding bulk samples but also exhibit many totally different properties (Dubertret et al., 2015). Because of their unique physical and chemical properties, such 2D materials have been attracted much attention for both of the fundamental scientific research and practical applications (Chhowalla et al., 2015; Chia et al., 2015; Dubertret et al., 2015; Yang et al., 2015b). Graphene (GR), a monolayer of sp^2-bonded carbon atoms arranged in honeycomb lattice, is a typical 2D material for carbon materials (Mas-Balleste et al., 2011). In 2004, Geim and co-workers at the University of Manchester developed a very simple methodology (the so called scotch-tape technique) to isolate the GR, which allowed them to first produce and characterize few-layers GR on silicon wafers (Novoselov et al., 2004). Following this pioneering work, several physical and chemical methods have been developed for the production of GR, including the intercalation and chemical exfoliation of graphite, unrolling of carbon nanotubes (CNTs), chemical vapor deposition (CVD) or epitaxial growth, reduction of graphene oxide (GO) and other organic synthetic methods (Avouris and Dimitrakopoulos, 2012; Brownson et al., 2012; Cai et al., 2012; Cao et al., 2014; Chen et al., 2012a; Edwards and Coleman, 2013; Guo and Dong, 2011; Hummers Jr and

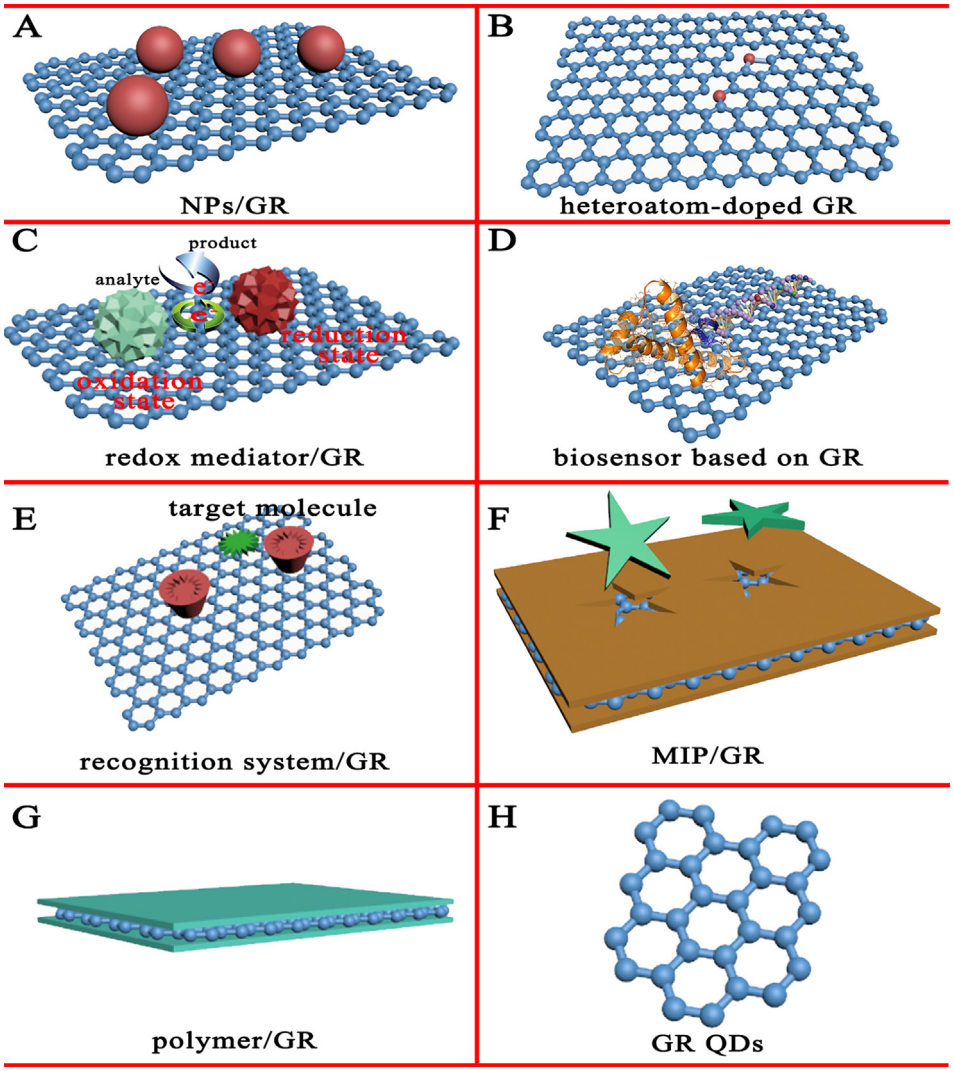

Fig. 1. Electrochemical sensors or biosensors based on NPs/GR (A), heteroatom-doped GR (B), redox mediators/GR (C), biomolecules/GR (D), recognition system/GR (E), MIP/GR (F), polymer/GR (G), and GR QDs (H).

Offeman, 1958; Loryuenyong et al., 2013; Mattevi et al., 2011; Yi and Shen, 2015). As a result of unique 2D structural property, GR is provided with a series of prominent intrinsic chemical and physical features, such as the quantum hall effect, high carrier mobility at room temperature (~10,000 $cm^2 V^{-1} s^{-1}$), large theoretical specific surface area (2630 $m^2 g^{-1}$), good optical transparency (~97.7%), high Young's modulus (~1 TPa) and excellent thermal conductivity (3000–5000 $W m^{-1} K^{-1}$) (Huang et al., 2012a). These excellent mechanical, electrical, and optical properties support GR as ideal building blocks in hybrid materials (Huang et al., 2012a). Since the direct observation and characterization of the mechanically exfoliated GR monolayer in 2004, GR has been highly anticipated to provide unique and new opportunities for wide applications in catalysis, batteries, supercapacitors, fuel cells, photovoltaic devices, photocatalysis, and electrochemical sensors and so on (Chen et al., 2012a; Georgakilas et al., 2012; Guo and Dong, 2011; Huang et al., 2012a; Liu et al., 2014d). As electrochemical sensors and biosensors, many advanced electrode interfaces were constructed through modification of electrode surface with GR or its composites, which can effectively decrease the overpotential and enhance the current response (Favero et al., 2015; Kochmann et al., 2012; Lawal, 2015; Pumera, 2009; Pumera et al., 2010; Shao et al., 2010; Vashist and Luong, 2015). Since GR was employed as the electrode materials for electrochemical sensing and biosensing for the first time in 2008 (Shang et al., 2008), GR-based electrochemical sensors and biosensors have been widely reported and applied in various analytical fields such as environment monitor, food security, and disease diagnosis (Antiochia and Gorton, 2014; Baptista et al., 2015; Chia et al., 2015; Feng and Liu, 2011; Kochmann et al., 2012; Kuila et al., 2011; Liu et al., 2014d; Pumera et al., 2010; Sajid et al., 2016; Shao et al., 2010; Song et al., 2016; Valentini et al., 2012; Wu et al., 2013; Zhou and Guo, 2015). In 2008, Papakonstantinou and co-workers reported the application of GR-based electrochemical sensor for the selective detection of dopamine (DA) in the presence of ascorbic acid (AA) and uric acid (UA) for the first time (Shang et al., 2008). Such work established that graphitic edge planes/defects are essentially responsible for the fast electron-transfer (ET) kinetics and excellent sensing and biosensing performance. Following the observation of high electrocatalytic performance of GR, many GR-based composites were also employed as electrode materials for electrochemical sensor and biosensor fabrication. In addition, by modifying nanoparticles (NPs) on GR support, the electrochemical performance of GR-based sensors and biosensors can usually be dramatically improved (Fig. 1(A)). For example, Fe_3O_4 magnetic NPs exhibited relatively low activity towards the electrocatalysis of hydrogen peroxide (H_2O_2), DA, or nitrite. However, the electrocatalytic activity of GR-Fe_3O_4 composite was greatly enhanced when Fe_3O_4 NPs were grown on GR support (Teymourian et al., 2013), which was attributed to the favorable chemical and electronic coupling between GR and Fe_3O_4 NPs because of the synergistic effect between them. Similarly, solution-grown CeO_2 NPs-GR composite (Hu et al., 2015), TiN NPs-GR composite (Wen et al., 2011), and electrodeposited Ni_2O_3/NiO NPs-GR composite (Liu et al., 2014a) all exhibited enhanced activity towards target molecules/biomolecules. Besides the NPs decoration, heteroatom-doping method was used to enhance the electrocatalytic activity of GR (Fig. 1(B)) (Bo et al., 2013; Sheng et al., 2012; Wang et al., 2010), which would be ascribed to the abundant edge plane like-sites/defects effectively introduced by incorporation of foreign atoms. In addition, redox mediators (such as hemin (Guo et al., 2011b) and organic dye (Song et al., 2012)) have been used to achieve "indirect" but enhanced electrocatalysis (Fig. 1(C)). The heterogeneous ET between the electrode and analyte is accelerated by the redox mediators which catalyze the electron exchange between the analyte and the electrode. Along with these strategies

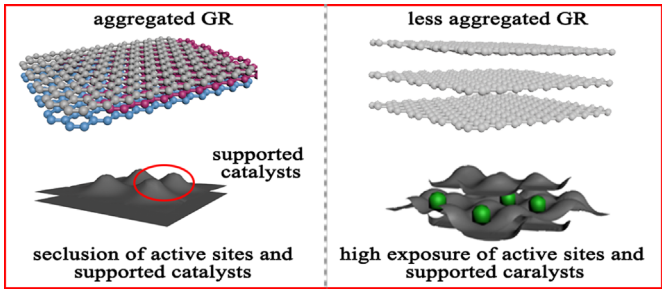

Fig. 2. The electrochemical properties of aggregated GR and less aggregated GR.

for improving the activity, some enzymes, proteins, antibodies, aptamers, and DNA have been used to construct GR-based biosensors or aptasensors and increase the selectivity and activity (Fig. 1(D)) (Ping et al., 2015; Song et al., 2016). Recently, it has been reported and confirmed that the incorporation of host-guest recognition system (cyclodextrin (CD) (Guo et al., 2010b) or calixarenes (Zhou et al., 2013)) on GR exhibited more outstanding supramolecular recognition and much higher electrochemical response to the target molecules than those of GR (Fig. 1(E)). Additionally, in the recent years there has been an increasing interest in the modification of GR's surface with a molecularly imprinted polymer (MIP) to enhance selectivity (Fig. 1(F)) (da Silva et al., 2014). In addition, polymer wrapping is also an interesting method to modify the surface of GR with functional group and increase the performance of GR-based electrochemical sensors (Fig. 1(G)) (Qiu et al., 2012; Ruecha et al., 2014). In addition to the GR sheets, GR quantum dots (QDs) combine the structure and properties of 2D GR and 0D carbon dots, which endows them with some of the unusual properties of GR. Due to quantum confinement and edge effects, GR DQs showed advantages in electrochemical sensors or biosensors (Fig. 1(H)) (Ju and Chen, 2015; Ruecha et al., 2014). In the recent years, the researchers have witnessed the significant development of electrochemical sensors or biosensors based on GR and its composites. These recent reviews thoroughly summarized the progress of GR in electrochemical sensors or biosensors (Carbone et al., 2015; Kuila et al., 2011; Kumar et al., 2015; Liu et al., 2014d; Song et al., 2016; Wang and Dai, 2015; Yang et al., 2015a).

Although much progress has been achieved by using GR as electrode materials, GR sheets tend to stack together through the π-π interaction (Li et al., 2012b; Si and Samulski, 2008) (Fig. 2(A)). The surface of GR is then much affected by the overlapping of the sheets due to the irreversible aggregation, which negatively affects its applications in electrochemical studies. The irreversible stacking of GR sheets results in that active sites for electrocatalysis be easily filled between GR sheets or hidden inside the stacked GR, then being absent for catalysis. Due to the irreversible agglomeration, NPs or nanoscale materials supported on GR layers are easily sandwiched between aggregated GR sheets or secluded inside the stacked layers and the utilization efficiency of supported NPs is limited (Fig. 2(A)). Therefore, it is important to alleviate the aggregation of GR layers and increase the surface area of GR. More efforts are being applied in improving the electrochemical activity of GR-based electrochemical sensors, and these works focus much on intercalation of carbon nanomaterials, surface modification (noncovalently functionalized and covalently functionalized GR), and structural engineering. The lifting of the aggregation of GR sheets can facilitate the exposure of the active sites and effectively increase the catalytic activity of GR-based electrochemical sensors (Fig. 2(B)). Due to the dispersed structure and large surface area of GR, NPs supported on GR are not hidden by aggregated GR layers and are highly exposed to targets of interest (Fig. 2(B)). Compared with aggregated GR, electrochemical sensors or biosensors based

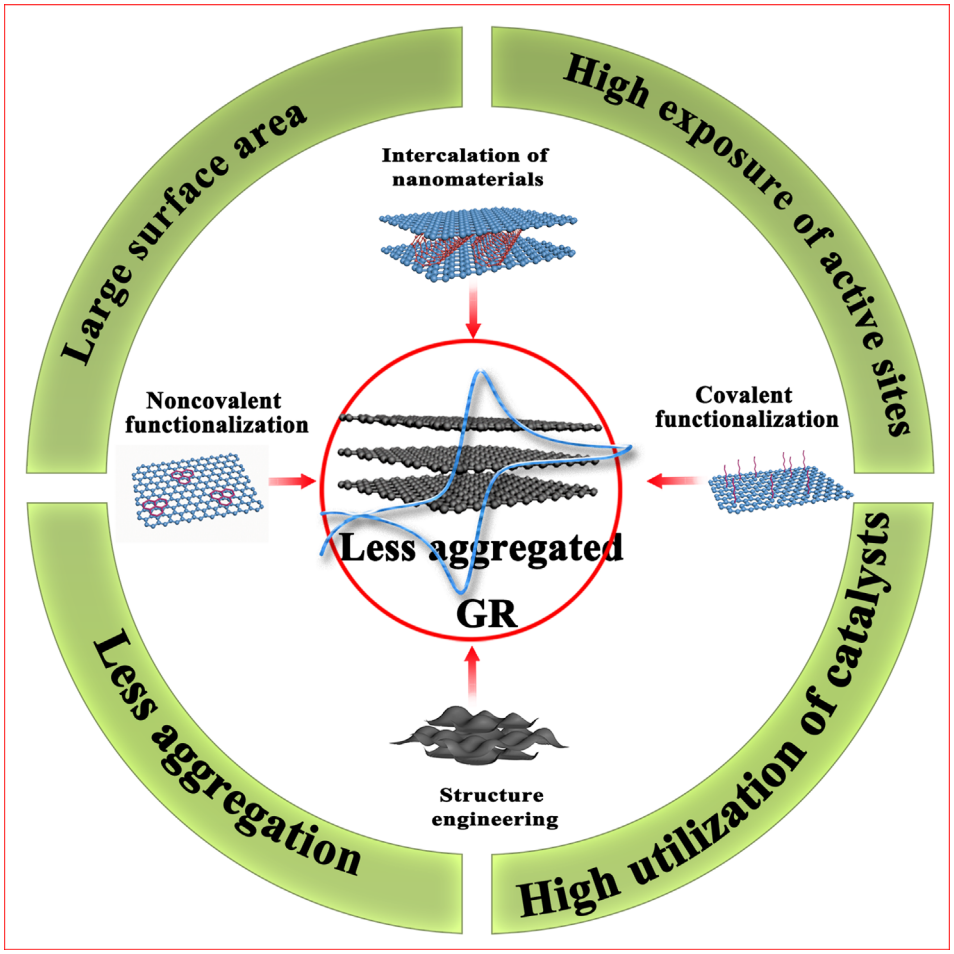

Fig. 3. Electrochemical sensors or biosensors based on less aggregated GR and their composites.

on less aggregated GR exhibit their own special advantages: (1) the high surface area of less aggregated GR favors the exposure of active sites; (2) the dispersed structure of less aggregated GR results in fast mass transport for reactant and product; (3) the large surface area and high dispersion of less aggregated GR provide more active sites for the growth of NPs, which facilitates the formation of highly dispersed and strongly bound metal phases. These properties make less aggregated GR to be very attractive for electrochemical sensing applications.

The present review summarizes recent advances and new progress for the development of electrochemical sensors based on less aggregated GR and its composites. Particular attention is given to intercalation of carbon nanomaterials, noncovalent functionalization and covalently functionalization of GR, and structural engineering for GR in the design of high-performance electrochemical sensors or biosensors (Fig. 3). Finally, current challenges along with future perspectives on the use of less aggregated GR for the rational design of electrochemical sensors are proposed.

2. Electrochemical sensors and biosensors based on less aggregated GR

2.1. Carbon nanomaterials/GR composites

Similar to the other 2D materials, the isolated GR sheets tend to aggregate together due to the van der Waals forces (Si and Samulski, 2008). After the aggregation, some of the unique advantages of 2D materials such as high surface area and high density of active sites are lost (Si and Samulski, 2008). To extend the applications of GR, much effort has been devoted to alleviate or minimize the aggregation of GR sheets. In 2009, Dai's group reported that CNTs/GR composite with the hierarchical structure was prepared by layer-by-layer (LBL) electrostatic self-assembly of poly(ethyleneimine)-functionalized GR sheets and acid-treated CNTs. The obtained CNTs/GR showed high performance as a capacitor (Yu and Dai, 2009). Following this work, they further developed a novel strategy for creating the 3D pillared vertically aligned CNTs (VACNTs)/GR architecture by an interesting intercalated growth of VACNTs into thermally expanded highly ordered pyrolytic graphite (Du et al., 2011). The rational combination of graphite allotropes, CNTs and GR leads to the formation of hybrid carbon films with interconnected carbon structures of well-defined nanoscale pores. Interestingly, the CNTs can bridge the defects for ET and increase the layer spacing between GR sheets. The VACNTs/GR architecture with a controllable nanotube length showed a high specific capacitance and remarkable rate capability. The attachment of CNTs spacers between GR sheets leads to the formation of hierarchical composites that can take full advantages of each kind of material.

As discussed above, the aggregation of GR can be alleviated with CNTs by using CNTs as the spacers to increase the interlayer spacing between GR sheets. The CNTs/GR showed high performance as supercapacitor. Based on the same principles, introduction of CNTs between the GR layers can improved the analytical performance of GR-based electrochemical sensors. For example, by a simple mechanical mixing method, Chen and co-workers fabricated CNTs/GR with high surface area and multi-modal porous

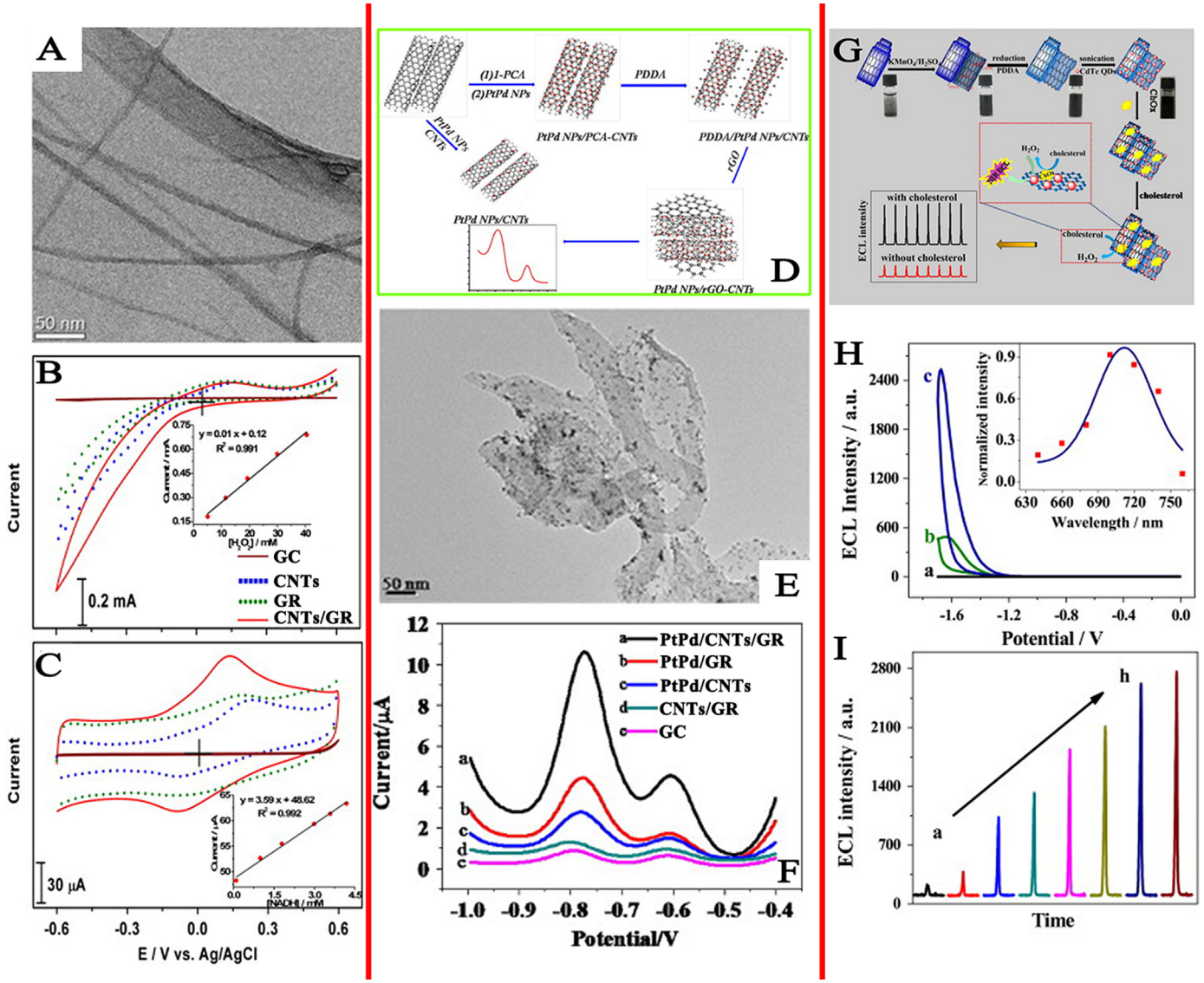

Fig. 4. (A) TEM image of GR/CNTs. CVs of (B) 40 mM H_2O_2 and (C) 4 mM NADH at GC modified with CNTs, GR, and GR/CNTs composite films in PBS. (D) The pathway for the synthesis of PtPd/CNTs/GR. (E) TEM image of PtPd/CNTs/GR. (F) Electrochemical detection of nitro compound at PtPd/CNTs/GR and other electrodes. (G) The schematic presentation for controllable preparation of CdTe/CNTs/GR for solid-state ECL cholesterol biosensor fabrication and its detection mechanism. (H) ECL-potential curves of bare GC (a), CdTe QDs/GC (b) and CdTe/CNTs/GR (c) in 0.10 M PBS with 50.0 μM H_2O_2. (I) ECL responses of ChOx/CdTe/CNTs/GR/GC in 0.10 M PBS in the presence of different concentration of cholesterol. (A-C) Reproduced with permission from Ref. Huang et al. (2013), Copyright 2013 Elsevier. (D-F) Reproduced with permission from Ref. Yuan et al. (2014a), Copyright 2014 Elsevier. (G-I) Reproduced with permission from Ref. Huan et al. (2015), Copyright 2015 Elsevier.

structure, which was applied as an electrochemical sensor for the detection of acetaminophen (APAP) (Chen et al., 2012c). Such sensor showed fast ET kinetics for APAP and exhibited excellent performance for the selective determination of APAP (with a low detection limit of 38 nM and a wide linear range of 0.05–64.5 μM) in the presence of DA in neutral solution. The long and tortuous CNTs were used to inhibit the aggregation of GR, which can significantly raise the electrolyte-accessible surface area in comparison with pure GR. In the subsequent work, Huang et al. compared the electrocatalytic activity of CNTs/GR with that of GR (Huang et al., 2013). The results from Raman spectroscopy, transmission electron microscopy (TEM) (Fig. 4(A)), atomic force microscopy (AFM), and scanning electron microscope (SEM) suggested that the CNTs can act as a conducting bridge to connect the isolated GR sheets, which would lead to the fast ET between the isolated GR sheets and is responsible for the high electrocatalytic activity of CNTs/GR. As an electrochemical sensor, the CNTs/GR showed high performance for H_2O_2 (red curve in Fig. 4(B)) and β-nicotinamide adenine dinucleotide (NADH) (red curve in Fig. 4(C)), reflecting the superior performance of CNTs/GR than GR as electrode material. The subsequent works similarly demonstrated the high activity and good analytical performance of CNTs/GR (Arvand and Gholizadeh, 2013; He et al., 2016; Niu et al., 2013; Prasannakumar et al., 2012; Qiu et al., 2016; Tran et al., 2014). Unlike the mechanical mixing of GR and CNTs, Prasannakumar used an LBL method to construct the CNTs/GR sensor through the alternative adsorption of the oppositely charged CNTs and GR (Prasannakumar et al., 2012). Additionally, unzipping few-walled CNTs (Zhu et al., 2014) and gamma radiations (Shahriary et al., 2014) were used as alternative methods for preparing CNTs/GR composites. Both composites also showed superior performance towards the analytes of interest. Besides CNTs, carbon nanofibers (Ye et al., 2013), hollow carbon spheres (Shahrokhian et al., 2014; Zhang et al., 2013), and macroporous carbon (Bo and Guo, 2013) can also prevent the irreversible aggregation of GR sheets and improve the analytical performance. In order to further boost the activity of CNTs/GR

composites, conductive ionic liquid (IL) was introduced (Niu et al., 2013). Due to the specific characteristics of IL, such as high ionic conductivity, wide electrochemical windows and good electrochemical stability, IL has been widely used in the field of electroanalysis (Ho et al., 2014; Shiddiky and Torriero, 2011). The combination of CNTs/GR and IL may bring out new properties and endow GR with high electrocatalytic activity. For example, in 2013, Niu et al. reported the preparation of 3,4,9,10-perylene tetracarboxylic acid (PTCA)-functionalized CNTs/GR/IL quaternary composites (Niu et al., 2013). Because of synergetic effects of conductive functionalized GR, CNTs, and biocompatible IL, the direct ET between DA and electrode surface can be efficiently achieved.

The introduction of metal NPs also further extends the applications of CNTs/GR as electrochemical sensors or biosensors. The porous structure of CNTs/GR provides larger surface area and more opportunity for the exposure of supported NPs. Compared with the aggregated GR, the electrocatalytic activity of NPs supported on CNTs/GR is effectively increased accompanied with the high utilization efficiency of NPs. For example, PtPd NPs supported on CNTs/GR exhibited high activity towards the nitro aromatic compound electroreduction compared with PdPd supported on CNTs or GR (Yuan et al., 2014a) (Fig. 4(D)). SEM confirmed the porous structure of CNTs/GR. TEM suggested that the PdPd NPs with the size of 1.2–3 nm were uniformly distributed on the framework of CNTs/GR (Fig. 4(E)). By comparing the electrochemical behaviors of nitro aromatic compound at different electrodes, a significant enhancement in the peak current was observed with the PtPd/CNTs/GR (curve a in Fig. 4(F)) which indicated the importance of the high surface area and porous structure of CNTs/GR in supporting the NPs. Similarly, iron NPs-decorated CNTs/GR showed high electrocatalytic activity towards electro-oxidation of nitrite and enabled good analytical performance (Mani et al., 2013b). Additionally, $Ni(OH)_2$ (Gao et al., 2014), Ni-Al layered double hydroxides (Fu et al., 2015), Pt NPs (Badhulika et al., 2014), and PtAu NPs (Lu et al., 2013b) supported on carbon materials/GR also exhibited efficient electrocatalytic activity for targets of interest. Very recently, an amplified solid-state electrochemiluminescence (ECL) biosensor for detection of cholesterol was constructed based on CdTe QDs decorated CNTs/GR composites (Fig. 4(G)) (Huan et al., 2015). In this case, CdTe QDs-decorated CNTs/GR nanoribbons were prepared by electrostatic interactions, which showed amplified ECL intensity and decreased onset potential compared with the pure CdTe QDs. The ECL intensity of CdTe QDs/CNTs/GR film was increased ~4.5 times over that of CdTe QDs, and the ECL onset potential of CdTe QDs/CNTs/GR modified electrode was positively shifted for ~100 mV than that of CdTe QDs (Fig. 4(H)). This fact suggested that the CNTs/GR in the CdTe QDs/CNTs/GR could enhance the ECL intensity of CdTe QDs and decrease the ECL onset potential effectively. By immobilizing cholesterol oxidase (ChOx) on the CdTe QDs/CNTs/GR, the as-prepared biosensor exhibited excellent performance for cholesterol detection including good reproducibility, selectivity, and acceptable linear range from 1 μM to 1 mM with a relative low detection limit of 0.33 μM (Fig. 4(I)). Importantly, this cholesterol sensor was successfully used to determine cholesterol in biological fluid and food sample.

Besides the electrocatalytic activity, the electrochemical sensors with high selectivity are also preferred. Along with the NPs decoration to boost the analytical performance of carbon material/GR composites, the enzymes and proteins have been used to increase both the selectivity and activity. CNTs/GR composites possess large specific surface areas and dispersed structure, which is an important prerequisite for the adsorption of enzymes. In 2013, Chen's group investigated the direct electrochemistry of glucose oxidase (GOx) at an electrochemically reduced GO/CNTs hybrid (ERGO/CNTs) (Mani et al., 2013a). The cyclic voltammograms (CVs) obtained at GOx/Nafion (a), ERGO/GOx/Nafion (b), CNTs/GOx/Nafion (c) and ERGO/CNTs/GOx/Nafion (d) film modified glassy carbon (GC) electrode in 0.1 M phosphate buffered saline (PBS) are presented in Fig. 5(A). The large peak current and low peak separation reflected GOx immobilized on ERGO/CNTs exhibited enhanced direct electrochemistry comparted with the GOx immobilized on CNTs or ERGO. In this case, strong interaction between CNTs and ERGO and porous structure leads to a synergistic enhancement of electrocatalytic activity of GOx. Then, the proposed glucose sensor based on ERGO/CNTs/GOx/Nafion exhibited low detection limit of 4.7 μM with wide linear range of 0.01–6.5 mM and acquired excellent storage and operational stabilities. Moreover, the activity of GOx/CNTs/GR can be further boosted by incorporation of NPs (such as Au NPs (Fig. 5B and curve d in Fig. 5(C)) (Yu et al., 2014b) and ZnO NPs (curve d in Fig. 5(D)) (Hwa and Subramani, 2014) into the framework of CNTs/GR. Other biomolecules whose adsorption on CNTs/GR have been also studied, including acetyl cholinesterase (Nayak et al., 2013), hemoglobin (Sun et al., 2013; Wang and Zheng, 2012), horseradish peroxidase (HRP) (Sheng et al., 2011), and heme peptide (Komori et al., 2015). These biomolecules/CNTs/GR composites similarly exhibited high selectivity and activity for target analytes. In addition to these enzymes or proteins, CD was used as host-guest recognition system for selective determination of pollutant and drug (Lu et al., 2013a; Yi et al., 2016). Although CD with a hydrophobic inner cavity and a hydrophilic outer side exhibits high molecular selectivity, the water-soluble CD shows low stability at electrode surface. Unlike the incorporation of CD, in 2012, Xing et al. reported an MIP electrochemical sensor based on polypyrrole-sulfonated GR/CNTs for sensitive detection of tryptamine (Xing et al., 2012). The polypyrrole-sulfonated GR/CNTs possessed high selectivity and affinity for target molecule.

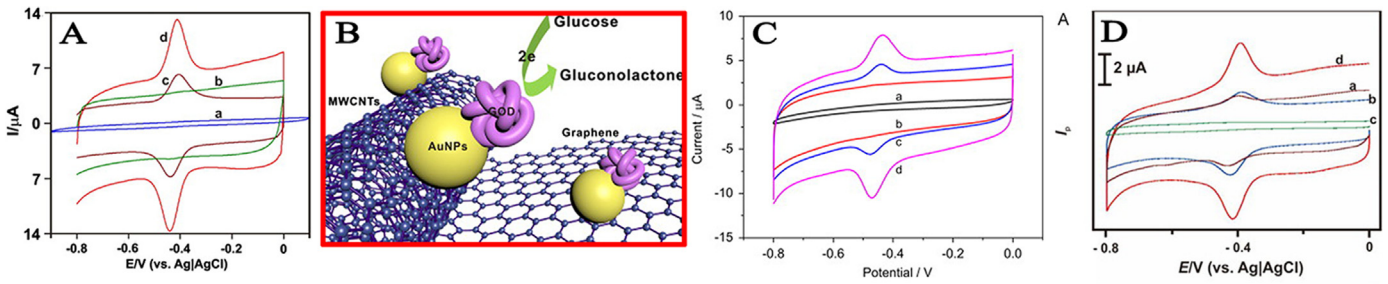

Fig. 5. (A) CVs obtained at (a) GOx/Nafion, (b) ERGO/GOx/Nafion, (c) MWCNT/GOx/Nafion and (d) ERGO/CNTs/GOx/Nafion film modified GCEs in PBS (pH 7). (B) Illustration of construction of GOx/Au NPs/CNTs/GR nanocomposites. (C) CVs of GOx (a), GOx/GR (b) GOx/CNTs/GR (c), GOx/Au NPs/CNTs/GR (d) film modified GCE in 0.1 M PBS. (D) CVs obtained at GOx/GR (a), GOx/CNT (b), GOx/ZnO (c) and GOx/ZnO/CNTs/GR (d) film modified GC in PBS. (A) Reproduced with permission from Ref. Mani et al. (2013a), Copyright 2013 Elsevier. (B and C) Reproduced with permission from Ref. Yu et al. (2014b), Copyright 2014 Elsevier. (D) Reproduced with permission from Ref. Hwa and Subramani (2014), Copyright 2014 Elsevier.

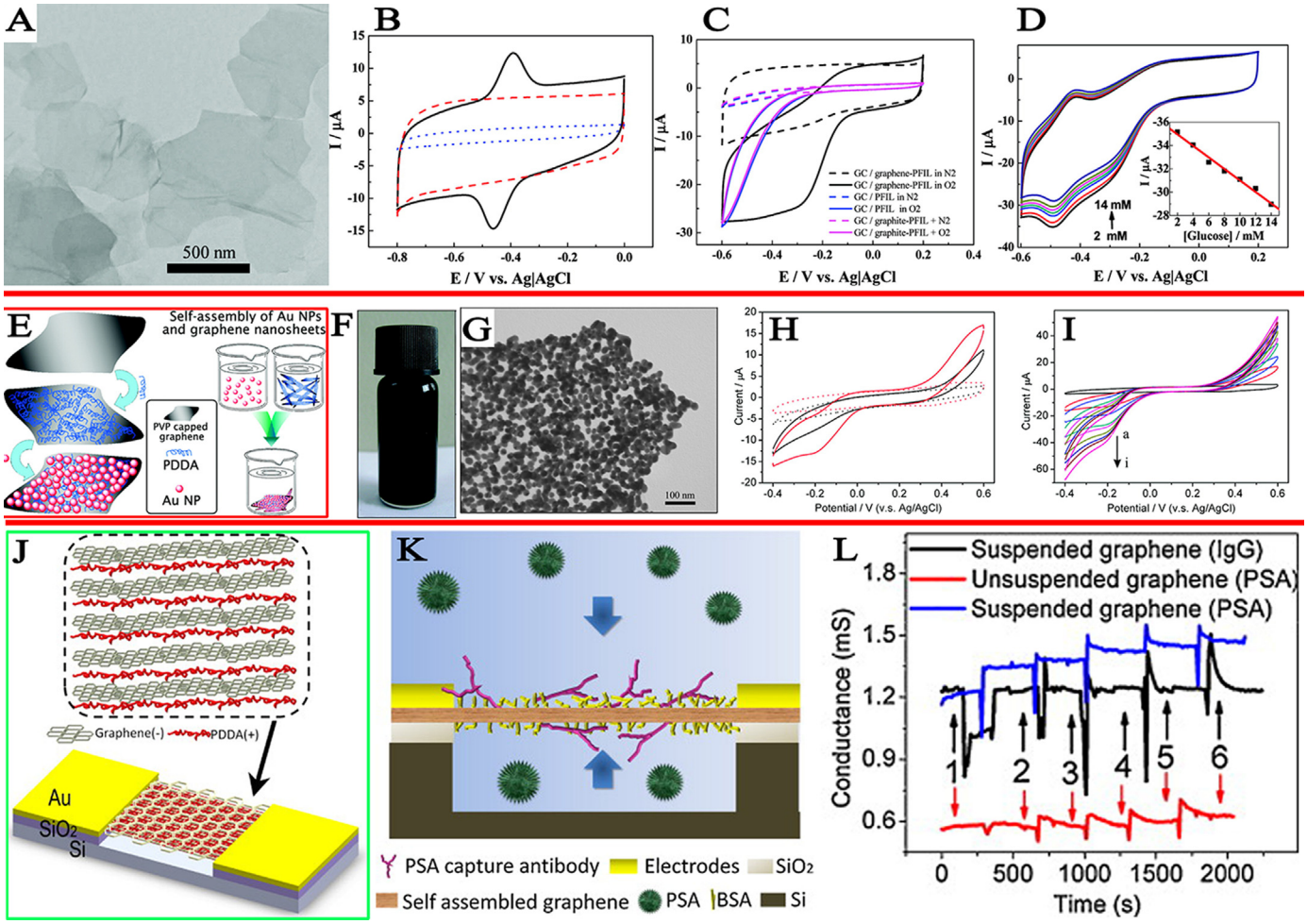

Fig. 6. (A) TEM image of PVP-protected GR. (B) CVs of GR/PFIL (dashed), graphite/GOx/ PFIL (dotted), and GR/GOx/PFIL (solid) modified electrodes in 0.05 M PBS. (C) CVs at PFIL (blue), graphite/PFIL (magenta), and GR/PFIL (black) modified electrodes in 0.05 M PBS solution saturated with O_2 (solid) and degassed with pure N_2 (dashed). (D) CVs of GR/GOx/PFIL modified GC electrode in various concentrations of glucose PBS solution. (E) Procedure for the self-assembly of Au NPs and PDDA-functionalized GR nanosheets. (F) Optical photographs of the PDDA/GR dispersion. (G) TEM images of GR/Au NPs. (H) CVs of the GR/Au NPs (red) and Au NPs (black) in the absence (dot) and presence (solid) of 1 mM H_2O_2 in 0.1 M PBS. (I) CVs of GR/Au-NPs in the N_2-saturated 0.1 M PBS with different concentrations of H_2O_2. (J) Sketch of suspended LBL self-assembled GR sensor structure and the self-assembled GR serves as the conducting channel bridging the electrodes of a biosensor. (K) Schematic illustration of immunoreaction between prostate specific antigen (PSA) capture antibodies and target protein PSA. (L) Conductance versus time for suspended and unsuspended GR with different concentrations of PSA solutions. (A-D) Reproduced with permission from Ref. Shan et al. (2009b), Copyright 2009 American Chemical Society. (E-I) Reproduced with permission from Ref. Fang et al. (2010), Copyright 2010 American Chemical Society. (J-L) Reproduced with permission from Ref. Zhang et al. (2012a), Copyright 2012 Elsevier. (For interpretation of the references to color in this figure legend, the reader is referred to the web version of this article.)

2.2. *Surface-functionalized GR*

As discussed above, the aggregation of GR limits its applications in electrochemistry. Recently, it has been demonstrated that the surface functionalization (non-covalent or covalent method) of GR can prevent the aggregation of GR layers (Georgakilas et al., 2012; Shan et al., 2009b). In addition, many electrochemical sensors utilizing GR sheets require surface modification of GR to make them more amenable to rational and predictable manipulation.

2.2.1. *Noncovalently functionalized GR*

Non-covalent functionalization of CNTs with polymers or polyelectrolytes through π-π interactions is an attractive synthetic method to make CNTs more dispersed in solvent and avoid stacking, because it offers the possibility of attaching functional groups to CNTs without disturbing the electronic network (Byrne and Gun'ko, 2010; Karousis et al., 2010). In the same manner, polyelectrolytes, such as poly (diallyldimethylammonium chloride) (PDDA) (Fang et al., 2010, 2012; Liu et al., 2010a; Xue et al., 2011; Zhang et al., 2011a), polyvinylpyrrolidone (PVP) (Shan et al., 2009b; Wajid et al., 2012), poly(allylamine hydrochloride) (Rotariu et al., 2014), and poly[(2-ethyldimethylammonioethyl methacrylate ethyl sulfate)-co-(1-vinylpyrrolidone)] (PQ11) (Liu et al., 2010b) have been used to noncovalently functionalize GR sheets. Moreover, these polyelectrolytes possess excellent binding capability with GR and could maintain the electronic structure of GR. After the functionalization, the electrostatic repulsion of the resulting charged polyelectrolyte/GR composites prevents the stack of GR layers. Accordingly, functionalizing GR with polyelectrolyte could be an effective method to increase the solubility and extend applications in biosensing. In 2009, Shan et al. reported the noncovalent functionalization of GR sheets with PVP (Shan et al., 2009b). It was found that PVP-protected GR was dispersed well in water. The TEM of PVP-protected GR showed the flake-like structure of GR (Fig. 6(A)). Using GOx as an enzyme model, a novel glucose sensor was constructed based on PVP-protected GR/polyethylenimine-functionalized IL/GOx (GR/PFIL/GOx). The GR-based composites achieved the direct ET of GOx and maintained its bioactivity well (Fig. 6(B)). The composites of GR/PFIL had good electrochemical reduction towards O_2 and H_2O_2 (Fig. 6(C)). Based on the high activity towards the O_2, a glucose biosensor was developed. Fig. 6(D) showed CVs of the obtained glucose biosensor

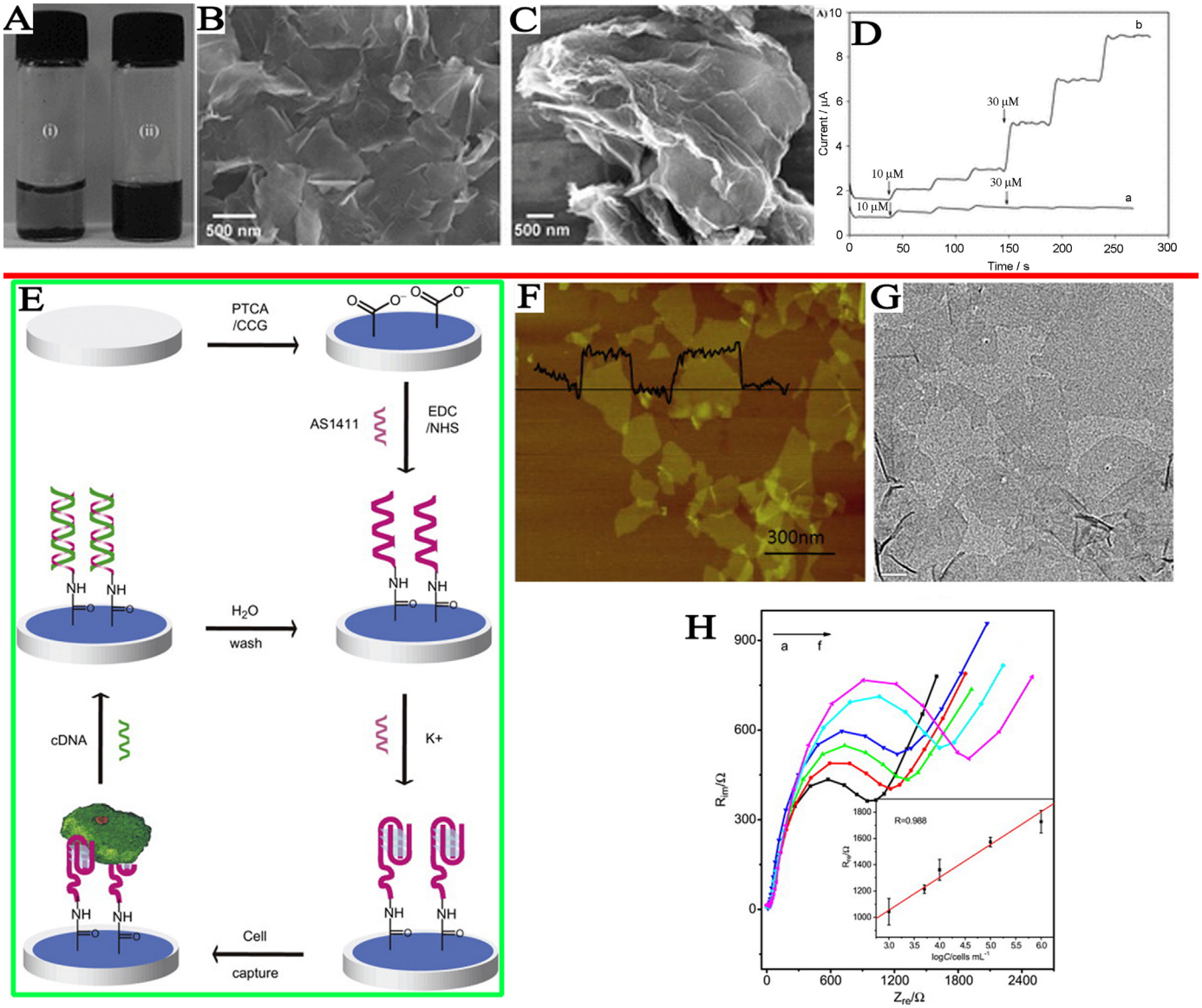

Fig. 7. (A) Photographic images of (i) GR, and (ii) SDBS-functionalized GR in water. SEM images of (B) SDBS-functionalized GR and (C) GR. (D) Analytical performance of SDBS-functionalized GR (a) and HRP/SDBS-functionalized GR (b) towards the H_2O_2. (E) Schematic representation of the reusable aptamer/GR-based aptasensor. (F) AFM and (G) TEM images of PTCA/GR. (H) Electrochemical impedance spectroscopy curves of aptamer/GR-based aptasensor the after immersed in different concentration of HeLa cell. (A-D) Reproduced with permission from Ref. Zeng et al. (2010), Copyright 2010 Wiley-VCH Verlag GmbH & Co. (E-H) Reproduced with permission from Ref. Feng et al. (2011), Copyright 2011 Elsevier.

with different concentrations of glucose. The glucose biosensor showed a linear range from 2 to 14 mM (inset of Fig. 6(D)). In the similar way, the PVP also facilitated the growth of NPs, which extended the electroanalytical applications of PVP/GR composites (Gong et al., 2011; Shan et al., 2010; Su et al., 2011; Xu et al., 2011b). In subsequent work, Liu et al. reported the preparation of PQ11-functionalized GR (Liu et al., 2010b). From their observation, the noncovalent functionalization of GR with PQ11 leads to highly dispersed GR that can be very stable for several months without any obvious floating or precipitated particles. As an Ag catalyst support, Ag NPs were deposited on the surface of GR using PQ11 as a reducing agent. An enzymeless H_2O_2 sensor was developed using Ag/PQ11/GR composites as electrode materials. The sensor exhibited good analytical performance towards the reduction of H_2O_2, such as fast response time, wide linear detection range, and low detection limit. In addition to PVP and PQ11, PDDA is also widely used as polyelectrolyte for noncovalent functionalization of carbon materials (Leng et al., 2011; Wang et al., 2011a). In 2010, Wang's group demonstrated the use of cationic polyelectrolyte PDDA functionalized GR sheets as the building block in the self-assembly of Au NPs to enhance the electrochemical activity (Fig. 6(E)) (Fang et al., 2010). From their result, the PDDA/GR dispersion was stable without precipitation for even more than 1 month at ambient condition (Fig. 6(F)). They found that the use of PDDA not only altered the electrostatic charges of GR, but also probably provided a convenient self-assembly approach to the hybridization of GR. Furthermore, Au NPs with high loading amount were distributed on PDDA/GR (Fig. 6(G)). The obtained electrochemical materials exhibited high performance for H_2O_2 (Fig. 6(H) and (I)). Similarly, PDDA-functionalized GR or its derivatives showed good performance for APAP (Lu et al., 2012), eugenol (Feng et al., 2014), H_2O_2 (Jia et al., 2013), organophosphate pesticide (Wang et al., 2011b), UA (Xue et al., 2011), and metronidazole (Liu et al., 2013). The PDDA is positive charged polyelectrolyte, which is favorable for the LBL in the assembly. In 2012, Cui's group reported the fabrication of cancer sensor based on LBL films assembled by

alternate adsorption of PDDA/poly(styrene sulfonate) (PSS) and PDDA/GR onto a silicon wafer (Fig. 6(J) and (K)) (Zhang et al., 2012a). Suspended LBL self-assembled GR was demonstrated to provide a simple and effective way to synthesize an ultra-sensitive and label free sensor to detect cancer markers with a detection limit down to 0.4 fg ml^{-1} (Fig. 6(L)).

Besides the polyelectrolytes, some aromatic compounds were also reported for noncovalent functionalization of GR to alleviate the aggregation of GR layers and improve the electrocatalytic activity. For example, the negatively charged sodium dodecyl benzene sulfonate (SDBS) was used to functionalize GR sheets (Zeng et al., 2010). The SDBS-functionalized GR suspension appeared to be very homogenous and stable for 2 months (Fig. 7(A)). The SEM image showed that the SDBS-functionalized GR was well separated from each other (Fig. 7(B)). In contrast, SEM image of GR showed much thicker platelets (Fig. 7(C)). In addition, SDBS-functionalized GR with negative charged was easily assembled with positively charged HRP through the LBL methodology. The SDBS-functionalized GR can prevent the aggregation of GR layers. Meanwhile, well-dispersed GR sheets can provide flexible distance and restack by adapting to the dimensions of HRP biomolecules, which is important to retain the native conformations of the guest enzymes. The HRP/SDBS-GR electrode showed excellent electrocatalytic performance towards the reduction of H_2O_2 with fast response, wide linear range, high sensitivity, and good stability (Fig. 7(D)). In the same manner, the methylene green (MG) was used to noncovalently functionalize GR to form a new kind of electroactive nanocomposite (Liu et al., 2009). After the noncovalent functionalization, the positive charge of MG/GR avoided the aggregation of GR and thereby increased its dispersity in aqueous solution. Moreover, the successful attachment of MG onto GR not only solubilized the MG/GR nanocomposite into aqueous

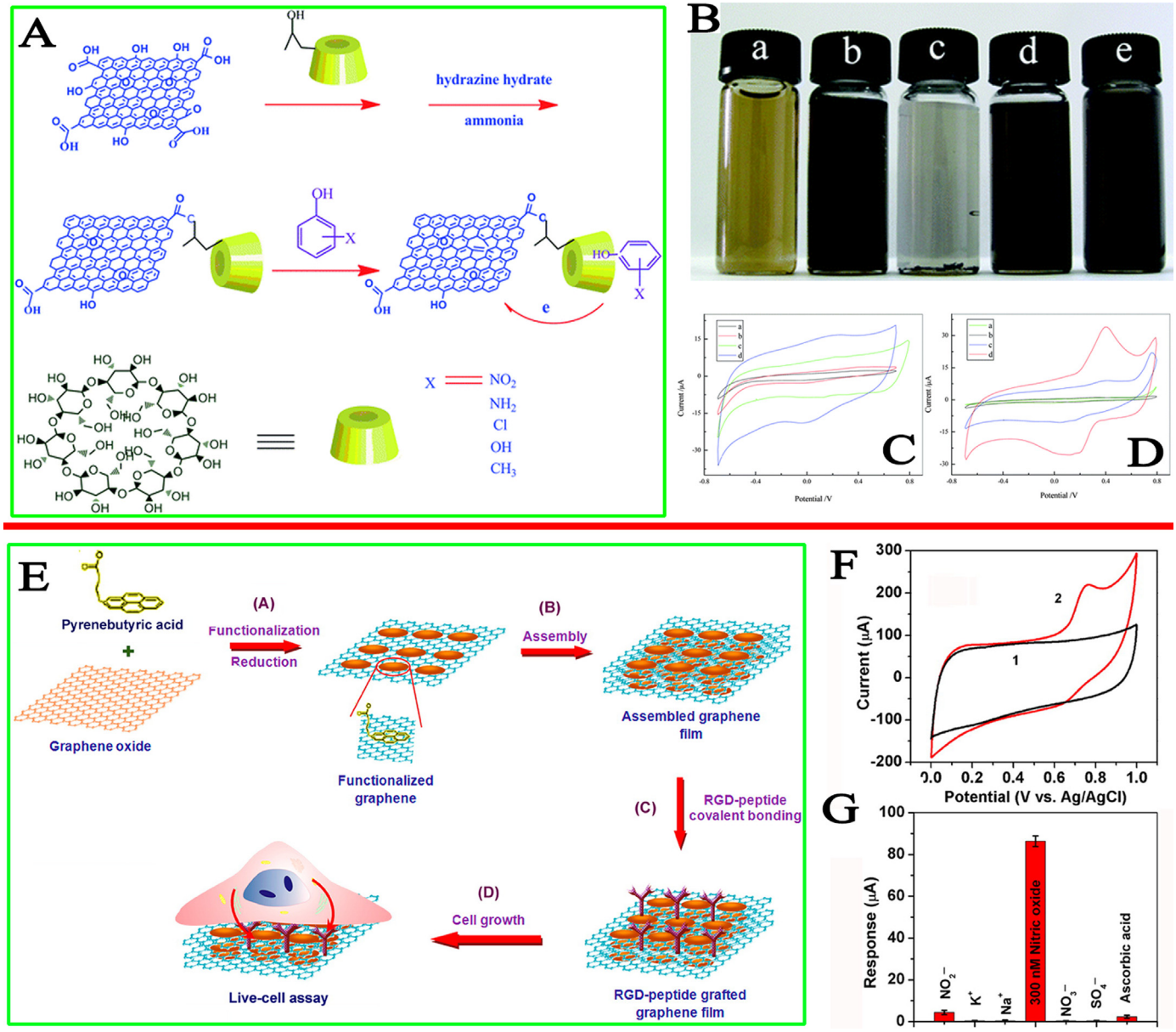

Fig. 8. (A) Schematic of the synthesis procedure of HP-β-CD/GR composites. (B) Optical photographs of GO (a), HP-β-CD/GR (b), and GR (c) dispersions in water and HP-β-CD/GR dispersions in DMF (d) and acetone (e). (C) CVs of 1 mM (C) o-nitrophenol and (D) 2,4,6-trichlorophenol at GC electrode (a), GO/GC (b), GR/GC (c), and HP-β-CD/GR/GC (d). (E) Schematic illustration of preparation of the free-standing biomimetic film and its live-cell assay. (F) CVs of the RGD-peptide covalently bonded GR film in cell culture medium in the absence (1) and presence (2) of 10 μM NO. (G) Selectivity of RGD-peptide covalently bonded GR film. (A-D) Reproduced with permission from Ref. Xu et al. (2011a), Copyright 2011 Royal Chemical Society. (E-G) Reproduced with permission from Ref. Guo et al. (2012), Copyright 2012 American Chemical Society.

media, but also endowed GR layers with excellent redox electrochemical property and electrocatalytic activity towards NADH oxidation. In another example, Feng and co-worker developed a facile and versatile method to increase the dispersion of GR via noncovalent functionalization of GR with PTCA (Feng et al., 2011). PTCA strongly adsorbed on GR through π–π interaction and hydrophobic interaction is used to avoid GR aggregation and introduce more negatively-charged -COOH groups on GR surface, without further destroying the conjugated π-system of GR (Fig. 7(E)). The result from AFM demonstrated that PTCA/GR sample separated well in single sheet with average topographic height of ~1.4 nm (Fig. 7(F)). The comparison of SEM and TEM image of PTCA/GR (Fig. 7(G)) and GR demonstrated that PTCA can effectively prevent the aggregation of GR layers. Furthermore, the nanocomposite was covalently functionalized with NH_2-modified nucleolin-specific aptamers as the recognition element. The binding amount of cancer cells can be quantitatively analyzed by the change of ET resistance of $[Fe(CN)_6]^{3-/4-}$ probe, because the cancer cells increases the ET resistance by blocking the access of the redox probe (Fig. 7(H)). In the similar way, pyrene-grafted poly (acrylic acid) (PAA)-functionalized GR was prepared through π-π interaction between GR and pyrene (Zhang et al., 2011b). The negative charged PAA prevents the GR from aggregating in solution after the final reduction stage of the GO, thereby yielding isolated sheets with improved water solubility. Using LBL method, a simple approach for GR/CdSe NPs multilayer films was developed to create a novel ET system, which is promising in the detection of thrombin. Other modifiers, such as thionine (Zhu et al., 2012), N-(trimethoxysilylpropyl) ethylenediamine triacetic acid (Hou et al., 2010), benzylamine (Liu et al., 2011), poly-L-lysine (Shan et al., 2009a), positively charged N,N-bis-(1-aminopropyl-3-propylimidazol salt)-3,4,9,10-perylene tetracarboxylic acid diimide (Hu et al., 2012) were also used as stabilizing agent to prevent the aggregation of GR layers and improve the analytical performance of GR-based electrochemical sensors and biosensors. These modifiers can effectively prevent the irreversible aggregation of GR layers in aqueous solution due to the electrostatic repulsion. It should be noted, however, the GR layers are more or less aggregated at the electrode surface when they dried at the electrode surface.

2.2.2. *Covalently functionalized GR composites*

Compared with the non-covalent surface modification discussed above, covalent functionalization methods offer a stronger linkage between the functional groups and GR. At the same time, the covalent functionalization of GR with organic molecules also effectively prevents the aggregation of GR layers (Georgakilas et al., 2012; Sudeep et al., 2013). Moreover, the covalent functionalization methods also provide additional advantages for controlling the linkage site and accessibility to the attached biomolecules, leading to an improved selectivity and stability for sensing and biosensing application. In addition, the covalent approaches possess some advantages such as stability and high surface coverage for further functionalization, compared with the non-covalent approaches. Covalent functionalization of GR has been achieved either through the formation of covalent bonds between free radicals or dienophiles and C=C bonds of pristine GR or the formation of covalent bonds between organic functional groups and the oxygen groups of GO (Dai, 2012; Dreyer et al., 2010). For instance, CD usually displays a selectively binding activity to many kinds of inorganic, organic and biological molecules into their cavities (Harada, 2001; Li and Purdy, 1992). Xu et al. showed that the hydroxypropyl-β-CD (HP-β-CD) was covalently grafted onto the surface of GR sheets via ester bonds (Fig. 8(A)) (Xu et al., 2011a). The functionalized GR was characterized by Fourier transform infrared, Raman, AFM, and thermogravimetric analysis. Furthermore, they provided additional evidence for the surface covalent modification of GR with CDs by solubility measurements. The solubility of HP-β-CD/GR could be readily observed after weeks later (Fig. 8(B)). It can be seen that no precipitation was observed for the HP-β-CD/GR nanocomposites in water. In contrast, the same amount of GR without surface modification began to precipitate immediately after sonication in water. By combining the recognition properties and conductive properties of GR, HP-β-CD covalently-functionalized GR exhibited outstanding supramolecular recognition and high electrochemical response to several phenolic organic pollutants, such as o-nitrophenol (curve d in Fig. 8(C)) and 2,4,6-trichlorophenol (curve d in Fig. 8(D)). This work demonstrated a new route to increase the selectivity of GR-based electrode and opened up the possibility of building more complex multicomponent nanostructures, which was believed to be useful for electrochemical sensors. Another interesting covalent modification of GR with peptide was reported by Li's group (Guo et al., 2012). They constructed smart functional biomimetic film sensor by covalently bonding RGD-peptide on pyrenebutyric acid-functionalized GR surface for real time electrochemical detection of nitric oxide (NO) molecule released from attached human cells under drug stimulations (Fig. 8(E)). The RGD-peptide covalently bonded GR biofilm showed a large oxidation peak with peak potential at 750 mV in cell culture medium containing 10 μM of NO (curve 2 in Fig. 8(F)), showing good electrocatalysis towards the oxidation of NO. As displayed in Fig. 8(G), the RGD-peptide grafted GR biofilm sensing matrix also had a good selectivity towards NO molecule and can eliminate the interferences. In addition, GR covalently bonded with NH_2-IL showed high dispersion in water. Moreover, the positively charged IL-functionalized GR sheets were strong enough to drive the formation of the 3D nanomaterials with negatively charged citrate-stabilized Pt NPs through electrostatic interaction (Zhu et al., 2010). Following the ultraviolet-visible spectroscopy, AFM, and CV result, a regular and uniform multilayer film was constructed and Pt NPs were uniformly adhered to the surface of the IL-GR within one bilayer through the electrostatic interaction. The developed LBL nanomaterials containing IL-GR and Pt NPs showed high electrocatalytic activity towards oxygen reduction. Furthermore, the electrocatalytic activity of the films could be further tailored by simply choosing different cycles in the LBL process. In the same manner, the positively charged IL-GR was alternately complexed with the negatively charged sulfonic acid functionalized GR (*s*-GR) through an electrostatic LBL process (Gu et al., 2012). The obtained $[IL\text{-}GR/(s\text{-}GR)]_n$ showed high activity towards the reduction of H_2O_2. After further immobilization of GOx on $[IL\text{-}GR/(s\text{-}GR)]_n$ film, the resulting $[IL\text{-}GR/(s\text{-}GR)]_n$/GOx/Nafion biosensor displayed an excellent response to glucose at a potential of −200 mV. Combined with on-line microdialysis system, the glucose biosensor in the on-line system exhibited wide linear range from 10 μM to 500 μM and a low detection limit of 3.33 μM. In addition, the IL-GR also has been used as an enhanced material for rapidly electrochemical detection of trinitrotoluene with good analytical performance (Guo et al., 2011a). Similarly, neutral red covalently-functionalized GR sheets also exhibited high stability and solubility in different solvents and high activity towards the detection of UA (Song et al., 2012).

2.3. *Structural engineered GR*

Noting the GR layers tend to preferentially form aggregated structure to minimize the presence of edge plane sites, various structural engineering strategies, such as vertical structure (Akhavan et al., 2012), tube-like structure (Zhang et al., 2012b), and porous structure (Cao et al., 2013; Wang et al., 2014b; Yue et al., 2014), have been applied to proliferate the exposed edge

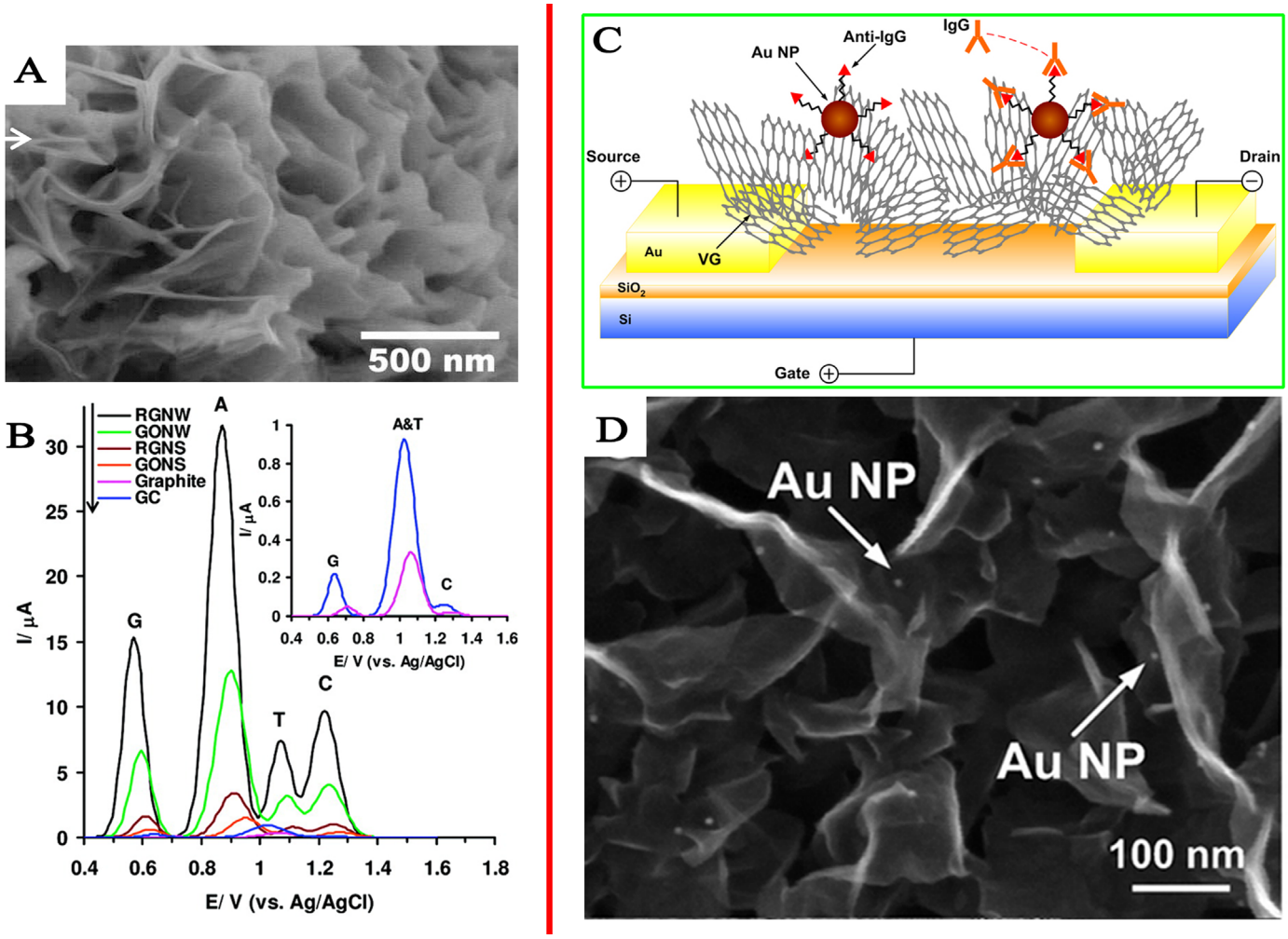

Fig. 9. (A) SEM images of the GR nanowalls. (B) DPV profiles of the RGNW, graphite, RGNS, GONW, and GC electrodes in an equimolar mixture of G, A, T, and C. (D) SEM image of vertically-oriented GR network deposited with Au NP-antibody conjugates. (A and B) Reproduced with permission from Ref. Akhavan et al. (2012), Copyright 2012 American Chemical Society. (C and D) Reproduced with permission from Ref. Mao et al. (2013), Copyright 2013 Nature Publishing Group.

sites of GR for enhanced electrocatalytic activity. The structural engineered GR and its composites have been widely used in the various fields because of large surface area and porous structure (Chabot et al., 2014; Han et al., 2014; Li and Shi, 2012; Y. Li and Shi, 2012; C. Li and Shi, 2012; Mao et al., 2015; Patil et al., 2015; Wang et al., 2015a; Xia et al., 2014; Yan et al., 2015). The increased distance between layers of structural engineered GR alleviates the aggregation of GR sheets and is favorable for the exposure of active sites for electrocatalysis (Akhavan et al., 2012). Many edge plane sites of aggregated GR layers are secluded inside the aggregated GR sheets, while they are exposed at the surface of structural engineered GR with large surface area (Wang et al., 2015a). The high exposure of defects within the structural engineered GR sheets can also generate more active edge sites for catalysis, increasing their performance (Dong et al., 2012b).

2.3.1. *Vertical GR*

As discussed above, the electrocatalytic activity may scale with the effective surface area of the GR. The role of GR structure in improving electrocatalytic performance has been clearly demonstrated through the comparison of reduced GR nanowall (RGNW) and reduced GR nanosheet (RGNS) towards the DNA detection in Akhavan's work (Akhavan et al., 2012). In this work, RGNW with extremely sharp edges and preferred vertical orientation was deposited on a graphite electrode by using electrophoretic deposition in an Mg^{2+}-GO electrolyte followed by hydrazine reduction. Then, the fabricated RGNW-electrode with large surface area and more edge plane defects was applied, for the first time, in developing an ultra-high-resolution electrochemical biosensor for detection of the four DNA bases. The SEM image in Fig. 9 (A) showed that the surface of the graphite electrode was covered with petal-like GR nanoflakes with lateral sizes of ~500 nm and extremely sharp edges (with 1–15 nm thickness at the edges). These GR nanoflakes exhibited random directions but with a preferred vertical orientation with respect to the substrate, which all resulted in the formation of a nest-like porous structure with a large surface area. After the reduction of GO with hydrazine, the nanowall structure of RGNW can be well retained. The extremely enhanced electrochemical reactivity of an equimolar mixture of G, A, T, and C with a concentration of 0.1 μM at the surface of the RGNW (black line in Fig. 9(B)) electrode was examined and compared to the electrochemical performance of RGNS, GO nanowall (GONW), graphite, and GC electrodes. The large discrepancy in activity between RGNW and RGNS is due to the availability of active sites for electrocatalysis. The aggregation of RGNS layers leads to the occlusion of active sites into stacked layers, while active sites are exposed at the surface of RGNW with large surface area and large layer distance. In the subsequent work, Mao et al. reported a sensitive and selective field-effect transistor biosensor based on vertically-oriented GR sheets labeled with gold NPs-

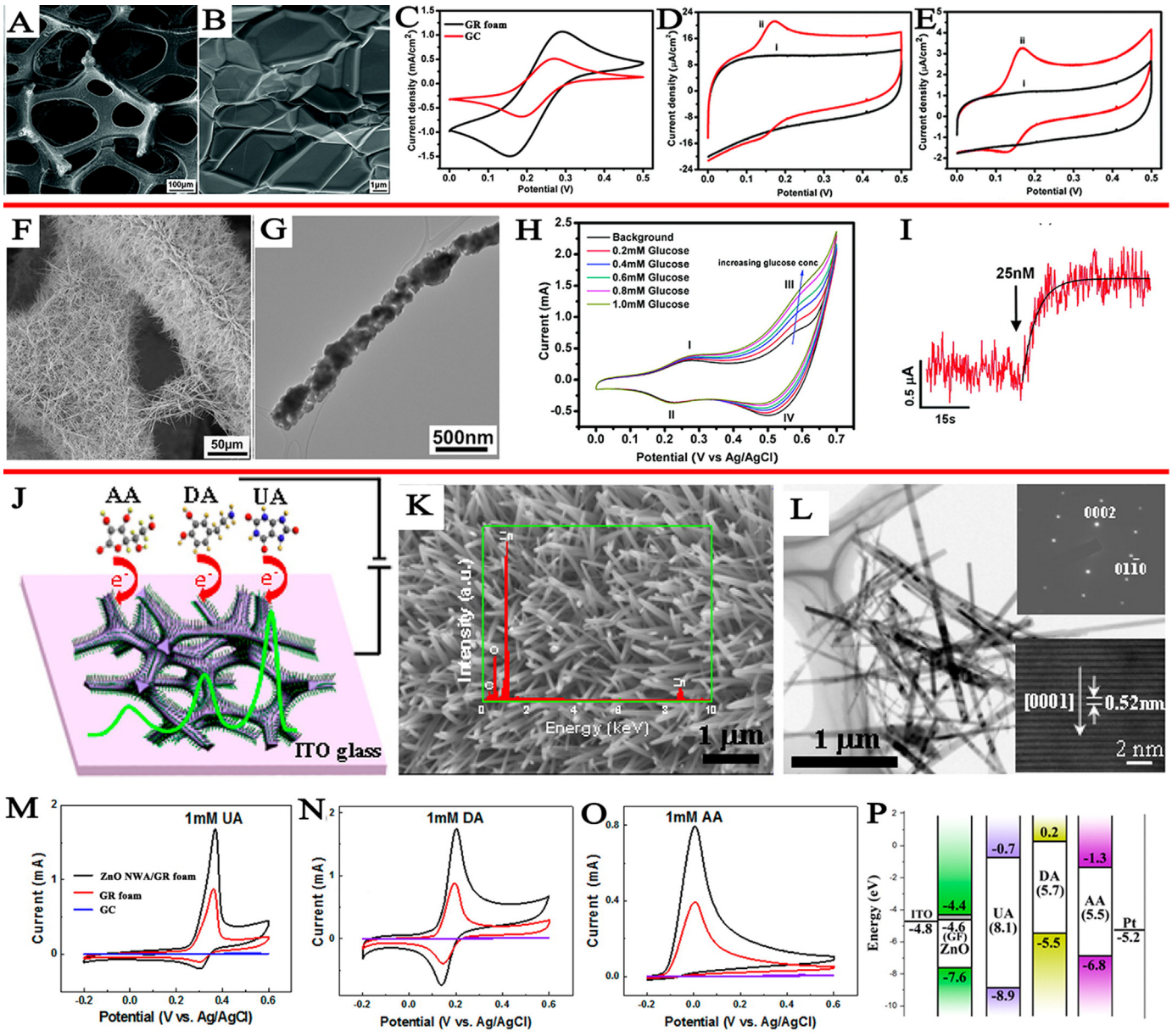

Fig. 10. (A) and (B) SEM images of GR foam at different magnification. (C) CVs of GC electrode (red) and GR foam electrode (black) in 5.0 mM $[Fe(CN)_6]^{3-/4-}$. CVs of (D) GR foam electrode and (E) GC electrode in PBS (i) without and (ii) with 20 μM DA. (F) SEM and (G) TEM images of Co_3O_4 nanowires/GR foam. (H) CVs of different concentration of glucose at GR foam. (I) Amperometric response to 25 nM glucose at GR foam. (J) Schematic of the ZnO NWA/GR foam electrode and detection of UA, DA, and AA. (K) SEM and (L) TEM images of ZnO NWA/GR foam. CVs of (M) UA, (N) DA, and (O) AA at ZnO NWA/GR foam (black), GR foam (red), and GC electrode (blue). (P) Flat band model (LUMO and HOMO) of the ZnO NWA/GR foam, UA, DA, and AA. (For interpretation of the references to color in this figure legend, the reader is referred to the web version of this article.) (A-E) Reproduced with permission from Ref. Dong et al. 2012c, Copyright 2012 American Chemical Society. (F-I) Reproduced with permission from Ref. Dong et al. (2012a), Copyright 2012 American Chemical Society. (J-P) Reproduced with permission from Ref. Yue et al. (2014), Copyright 2014 American Chemical Society. (For interpretation of the references to color in this figure legend, the reader is referred to the web version of this article.).

antibody conjugates (Fig. 9(C)) (Mao et al., 2013). In this work, vertically-oriented GR sheets were directly grown on the sensor electrode using a plasma-enhanced CVD method and function as the sensing channel. Based on the observation from the SEM and TEM, vertically-oriented GR sheets showed crumpled structure and were grown and accumulated from the bottom of the electrode. Moreover, HRTEM indicated that the vertically-oriented GR sheets have 4–6 layers. With a large specific surface area and a vertical structure, Au NPs-antibody conjugates were uniformly distributed and attached to the vertically-oriented GR surface (Fig. 9(D)) and the vertically-oriented GR-based field-effect transistor (FET) sensor showed a low detection limit, good specificity, and a short response time.

2.3.2. *Porous GR*

One early recognition of the role of real surface area in promoting the electrochemical performance of GR-based electrocatalyst was in supercapacitors system (Zhu et al., 2011), where researchers noted that the large specific surface area of chemical-activated GR afforded more available sites for charge accumulation. Following this work, different porous GR-based materials have been extensively designed, prepared and investigated for the practical applications in supercapacitors, lithium-ion batteries, gas adsorption, electrochemical biosensors, fuel cells, and solar cells with high performance from both fundamental and technological viewpoints (Gao and Duan, 2015; Han et al., 2014; Li and Shi, 2012; Li and Shi, 2012; Li and Shi, 2012; Mao et al., 2015; Patil et al., 2015; Wang et al., 2015a; Xia et al., 2014; Yan et al., 2015).

Among these synthesis methods, template-directed CVD is an important and easy method to prepare foam-like porous GR. The nickel foam is the mostly used template for the synthesis of GR foam and has been dominating in current literature. Chen et al. first reported foam-like GR using an interconnected nickel scaffold as template (Chen et al., 2011). Based on this pioneering work, the CVD method is widely used for preparation of GR foam and the CVD-grown GR is applied in different areas (Han et al., 2014; Wang et al., 2015a). Many demonstrations of improved performance through structural engineering of GR motivate the applications of porous GR in electrochemical sensors. For example, in 2012, Dong et al. demonstrated that macroporous, highly conductive, and monolithic GR foam synthesized by CVD can be used as a novel architecture for electrochemical sensors (Dong et al., 2012b). As shown in Fig. 10(A) and (B), GR foam exhibited well defined macroporous structure with the pore diameter of around 100–200 μm. The data from the N_2 adsorption-desorption isotherm showed that GR foam had a large specific surface area (~670 $m^2 g^{-1}$). The GR foam (black curve in Fig. 10(C)) showed fast ET for $[Fe(CN)_6]^{3-}/^{4-}$ probe compared with bare electrode (red curve in Fig. 10(C)). Compared with bare GC electrode (Fig. 10(E)), GR foam-modified electrode (Fig. 10(D)) displayed high electrocatalytic activity towards DA. As an electrochemical sensor for DA, they found that the porous GR foam can selectively detect DA with remarkable sensitivity and low detection limit. The authors believed that the high analytical performance of GR foam was attributed to the large surface area, fast mass transport, and high charge transfer rate of GR. In another notable study, it is found that the 3D GR foam exhibited poor voltammetric responses when compared to the freestanding 3D reticulated vitreous carbon due to the presence of hydrophobic behavior of 3D GR foam in aqueous media (Brownson et al., 2013; Figueiredo-Filho et al., 2014). Conversely, such 3D GR foam depicted favorable electrochemical characteristics when utilized as an electrode material in non-aqueous media (such as IL) towards some commonly employed redox probes. Subsequently, utilization of 3D GR nanoribbon foam prepared from silicon carbide foam by a high temperature and low vacuum process for electrochemical sensing applications was also reported by the same group (Brownson et al., 2016). The GR nanoribbon foam comprises on average 4 GR layers and shows a quasi-GR structure. In terms of the electroanalytical response of the 3D GR nanoribbon foam electrode, it is found to give rise to an improved linear range and limit of detection towards some analytes. However, in certain cases the alternative carbon based 3D foams (such as reticulated vitreous carbon and nickel foam- templated GR) out-performed the GR nanoribbon foam. Such result highlights that a compromise between heterogeneous electron transfer speed, the presence/absence of oxygenated species and the accessibility of the electrode's active surface area is required depending on the target analyte of interest. The porous GR shows high surface area and plenty of active sites, which is ideal for use as a scaffold for integration with other functional materials (such as, inorganic nanomaterial, antibody, or organic molecule) to generate synergistic effects.

Using porous GR as support, Zhang's group demonstrated that cobalt oxide (Co_3O_4) nanowires were in situ synthesized on porous GR foam through a simple hydrothermal procedure (Dong et al., 2012a). SEM and TEM indicated that the GR skeleton was fully and uniformly covered by the network of Co_3O_4 nanowires (Fig. 10 (F) and (G)). The Co_3O_4 nanowires/porous GR showed high performance as an enzyme-free ultrasensitive sensor of glucose because of the synergistic integration of the two novel nanomaterials (Fig. 10(H) and (I)). In their subsequent work, they also used the CVD-grown porous GR as the support for anchoring Pt NPs, CNTs and MnO_2 nanowalls and constructed electrochemical sensor to detect H_2O_2 based on the functionalized porous GR (Cao et al., 2013). Following the SEM and TEM observation, these nanomaterials can be well anchored on the surface of porous GR. Using H_2O_2 as probe molecule, the obtained functionalized porous GR materials exhibited high activity towards the oxidation of H_2O_2. Latterly, Yue et al. prepared vertically aligned ZnO nanowire arrays (ZnO NWA) on porous GR foam for selectively selective detection of UA, DA, and AA (Fig. 10(J)) (Yue et al., 2014). The SEM image in Fig. 10(K) exhibited the surface of the GR foam was fully covered by vertically aligned, highly uniform ZnO NWA. The single-crystallined ZnO with a lattice constant of 0.52 nm can be observed from by TEM image in Fig. 10(L). The signal amplification at the ZnO NWA/GR nanocomposites using several probes (UA in Fig. 10 (M), DA in Fig. 10(N), and AA in Fig. 10(O)) reflected the high electrocatalytic activity of ZnO NWA/GR compared to GR. The optimized ZnO NWA/GR foam electrode provided a high surface area and high selectivity with a detection limit of 1 nM for UA and DA. The insights from the authors informed that large surface area of porous GR foam structures, easily mass transport in the porous structure and high conductivity of GR foam, and more active sites of ZnO NWA surface were synergistically responsible for the high activity of ZnO NWA/GR foam-based sensors. Moreover, based on analysis of the gap between the lowest unoccupied molecular orbital and the highest occupied molecular orbital (LUMO-HOMO) of these biomolecules, the selectivity in the oxidation potential was explained by the gap difference between the LUMO-HOMO of a biomolecule for a set of given electrodes (Fig. 10(P)). In the similar manner, porous GR-supported Ag NPs (Zhan et al., 2014b), Mn_3O_4 nanomeshes (Si et al., 2013), ZnO nanorods (Dong et al., 2012a), Au NPs (Du et al., 2014), $NiCo_2O_4$ nanostructures (Wu et al., 2015), Ni $(OH)_2$ nanosheets (Zhan et al., 2014a), CuO nanoflowers (Ma et al., 2014), $Cu(OH)_2$ nanorods (Shackery et al., 2016), PtRu NPs (Kung et al., 2014), GOx (Liu et al., 2014b), polyoxometalate (POM) (Xu et al., 2015), and thionine (Xi et al., 2013) also exhibited excellent analytical performance towards the targets of interest. Besides the NPs decoration, the porous GR foam is promising for construction of immunosensor, because the large surface area and porous morphology improve the density, accessibility as well as the stability of the bioactive affinity ligands. For example, Liu et al. developed a high performance electrochemical immunosensor based on GR foam for sensitive detection of the tumor biomarker, carcinoembryonic antigen (CEA) (Liu et al., 2014a). HRP-labeled antibody was immobilized on the GR foam through the biospecific affinity of lectin with sugarprotein. The immunosensor was able to detect CEA with a wide linear range (0.1–750.0 ng ml^{-1}), low detection limit (~90 pg ml^{-1}), and short incubation time (30 min). The unique structural properties of GR foam ensured efficient mass transport and accessibility of bioaffinity ligands and provided high density of the immobilized antibody. By simply changing the respective antibodies, the proposed immunosensor can be extended for detecting other proteins. Additional works from the Kong's group also revealed that mesocellular GR foam using zeolite Ni-MCM-22 as the template can be used as advanced electrode materials for novel biosensor preparation (Li et al., 2014; Wang et al., 2014c). Although the CVD-grown GR foam is widely used in electrochemical sensors, GR foam prepared from CVD suffers from the involvement of an expensive machine.

In addition of CVD method, hard-template method has been a very common strategy for the preparation of porous GR structures because of its controllable pore size (Choi et al., 2012; Huang et al., 2012b; Meng et al., 2013). Polymer or inorganic particles can also serve as a hard template for the fabrication of porous GR. The self-assembly of GO onto the surface of template, reduction of GO, and the subsequent removal of template results in crumpled GR with pores that are originally occupied by the template species. The increased distance between porous layers effectively alleviates the aggregation of GR sheets. The active sites of nonporous GR are

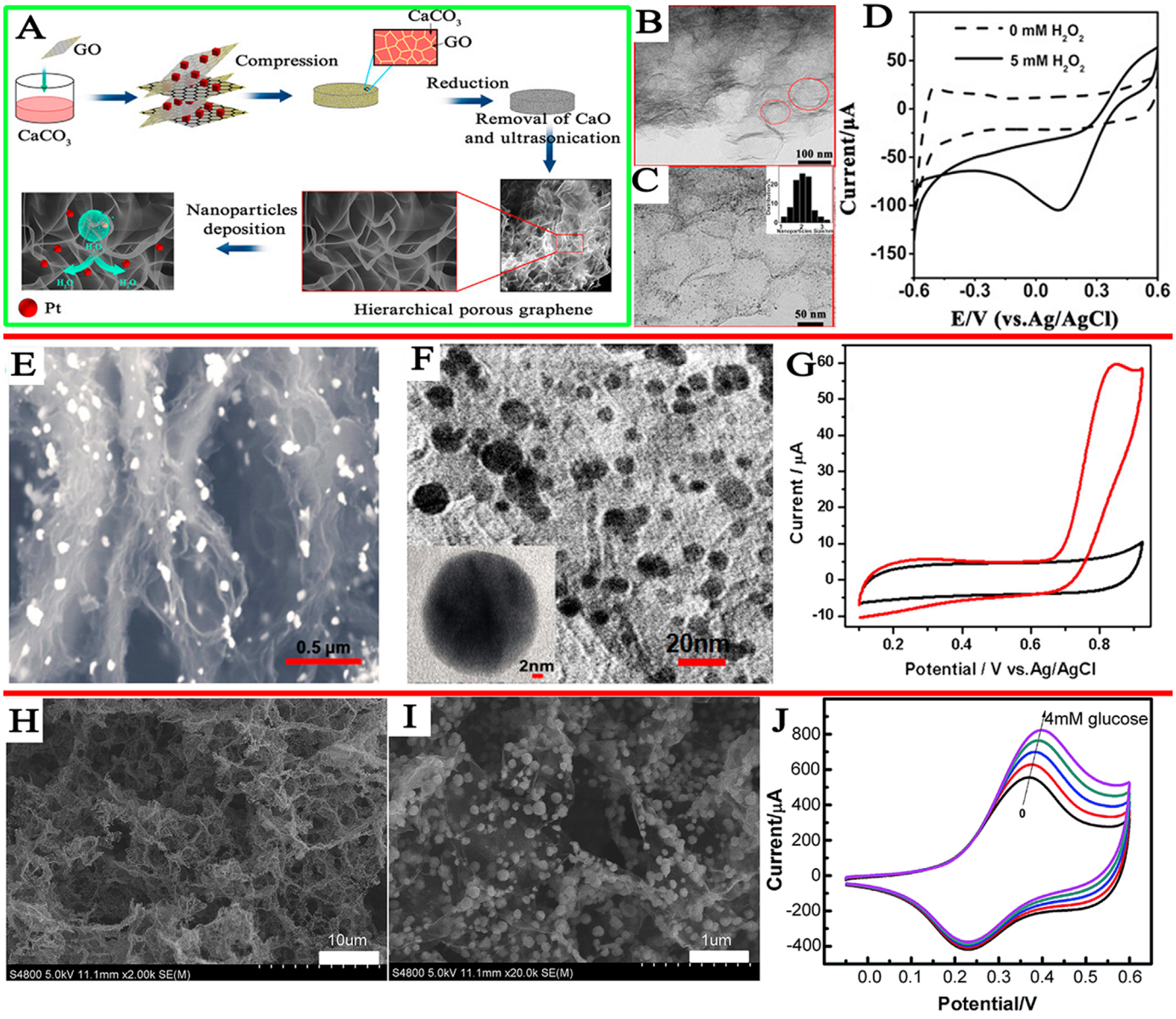

Fig. 11. (A) Illustration of the preparation of Pt/porous GR samples. TEM images of (B) porous GR and (C) Pt/porous GR. (D) CVs of Pt/porous GR in 0.1 M PBS containing 0 and 5 mM H_2O_2. (E) SEM and (F) TEM images of Au/GR hydrogels. (G) CVs of Au/GR hydrogels in 0.01 M PBS solution in the absence (black) and presence (red) of 0.5 mM NO. (H) and (I) SEM images of $Ni_{0.31}Co_{0.69}S_2$/GR hydrogels. (J) CVs of the $Ni_{0.31}Co_{0.69}S_2$/GR hydrogels modified electrode in 0.3 M NaOH solution with different concentrations of glucose. (A-D) Reproduced with permission from Ref. Li et al. (2015a), Copyright 2015 Elsevier. (E-G) Reproduced with permission from Ref. Li et al. (2015b), Copyright 2015 American Chemical Society. (H-J) Reproduced with permission from Ref. Li et al. (2015a), Copyright 2015 Royal Chemical Society. (For interpretation of the references to color in this figure legend, the reader is referred to the web version of this article.)

secluded inside the aggregated GR sheets, while the large surface area and porous structure of porous GR is favorable for the exposure of active sites for electrocatalysis. By engineering of GR to yield a high surface area and macroporous morphology, the active sites of GR have been dramatically increased, boosting its electrocatalytic performance. For example, Yu et al. developed a template-assisted self-assembly method to construct porous GR using polystyrene spheres as sacrificial template and hydrazine as reducing agent (Yu et al., 2014a). From the electrochemical data, the open porous structure and large surface area of porous GR notably enhanced the electrochemical properties of GR materials. A similar study reported by Guo's group compared the electrochemical performance of porous GR prepared from hard template and nonporous GR towards the simultaneous determination of hydroquinone, catechol, and resorcinol (Zhang et al., 2015a). The large discrepancy in electrochemical performance between porous GR and nonporous GR stemmed from the availability of the active sites for electrocatalysis. The high surface area of porous GR is favorable for the exposure of active sites for electrocatalysis and the porous structure is beneficial for mass transfer. In addition, the large surface area and porous structure of porous GR is suitable for the loading of NPs. When used as a support for NPs, the porous structure provides larger surface area and more opportunity for the exposure of supported NPs. For instance, Guo's group reported the synthesis of porous GR using commercial $CaCO_3$ as a hard template for the detection of H_2O_2 (Fig. 11(A)) (Liu et al., 2015a). Following the observation of SEM and TEM images (Fig. 11(B)), the micro-, meso- and macropores were found on the surface of porous GR sheets. During calcination, the $CaCO_3$ decomposed into CaO and CO_2, and CO_2 pushed and expanded the GO layers to enlarge the pores. The removal of CaO particles resulted into the formation of PGR with many macropores that were initially occupied by the

CaO particles. At the meantime, redox reaction between CO_2 and the carbon atoms of GR caused the cleavage of C-C bonds of GR and produced the micro- and mesopores. When used as a support for Pt NPs, Pt NPs were well dispersed and located on the surface of porous GR (Fig. 11(C)). From the electrochemical data, the Pt NPs supported on porous GR showed larger electrochemical active surface area and high activity towards the reduction of H_2O_2 compared with the Pt NPs supported on nonporous GR (Fig. 11(D)). This comparison evidently reflected the porous structure of porous GR is important for the exposure of supported NPs. In another works, the same group compared the electrochemical performance of CuO (Zhao et al., 2015) and Pt NPs (Zhang et al., 2016) supported porous and nonporous GR. Based on the same principle, the CuO and Pt NPs supported on porous GR showed high activity towards the detection of glucose and H_2O_2, respectively.

2.3.3. GR hydrogels or aerogels

Besides the template methods for the synthesis of porous GR above, template-free method is another important and easy method to prepare foam-like GR macrostructures with less aggregation and large surface area (Han et al., 2014; Wang et al., 2015a; Xia et al., 2014). Among these template-free methods, self-assemble hydrogel method is a simple, scalable, and environmental friendly method for the synthesis of porous GR (Nardecchia et al., 2013; Xu et al., 2010). Soluble GO with many functional groups (hydroxyl, epoxide, and carboxylic groups) provides the tethering sites for the linking of gelator molecules. After the hydrothermal process, the GO can be reduced to the GR accompanied with the formation of hydrogels. The macropores of GR hydrogels efficiently prevent the aggregation of GR layers. The GR hydrogels showed promising applications in catalysis, dye adsorption, and supercapacitor (Nardecchia et al., 2013). As electrode materials for electrochemical sensors, GR hydrogels have been attracted much attention recently. For example, Cai et al. reported the synthesis nitrogen-doped GR hydrogels using DA as cross-linkers and nitrogen source (Cai et al., 2016). The nitrogen-doped GR hydrogels showed high performance for the detection of H_2O_2. Similar conclusion is arrived at nitrogen-doped GR hydrogels for detection of adenine (Li et al., 2016). Very recently, Liu et al. employed the porous GR hydrogels as an excellent support for immobilizing microbe (Liu et al., 2015b). The size of porous GR hydrogels can be easily adjusted by changing the amount of neutral red. GR hydrogels were used as a support for immobilizing microbe, which showed ~3.3 times more load mass of microbe than commonly used supports and 2.5 times higher biodegradation efficiency than carbon fiber felt. GR hydrogels can provide large microbe/liquid interfaces, where water and other liquids can be easily accessed the interconnected porous structure. The biochemical oxygen demand sensor based on GR hydrogels exhibited a linear range of 2–64 mg O L^{-1} and a detection limit 0.4 mg O L^{-1} for glucose-glutamic acid. To further boost the performance of GR hydrogels, NPs are deposited on the framework of GR hydrogels. For example, Au decorated-GR hydrogels prepared by in situ reduction of Au^{3+} on GR hydrogels exhibited high performance for detection of NO released from living cells (Li et al., 2015b). The SEM and TEM images showed that the highly porous structure of GR hydrogels offered a large surface area for uniform deposition of Au NPs (Fig. 11(E) and (F)). The synergistic interaction between the Au NPs and GR hydrogels efficiently catalyzed the electrochemical oxidation of NO with excellent selectivity, fast response, and low detection limit (Fig. 11(G)). Similarly, in 2014, Zhang et al. reported the mixture of GO, 2,4,6-trihydroxybenzaldehyde, urea, and potassium hydroxide for the synthesis of nitrogen-doped activated GR aerogels. Potassium hydroxide activation generated large pores on the wall of the GR aerogels. The nitrogen-doped activated GR aerogels were used a support for Au NPs. The resulting Au NPs/nitrogen-doped activated GR aerogels offered excellent electronic conductivity (28,000 S m^{-1}), specific surface area (1258 m^2 g^{-1}), well-defined hierarchical porous structure. Owing to the greatly enhanced ET and mass transport, the developed sensor based on Au NPs/nitrogen-doped activated GR aerogels displayed an ultrasensitive electrochemical response to hydroquinone and o-dihydroxybenzene (Juanjuan et al., 2014). Using a different approach, Li et al. reported one-step method for the synthesis of $Ni_{0.31}Co_{0.69}S_2$/GR hydrogels as an enzyme-free sensor for glucose (Li et al., 2015a). From the SEM image, $Ni_{0.31}Co_{0.69}S_2$ NPs are uniformly located on the porous GR nanosheets (Fig. 11(H) and (I)). Benefitting from the excellent redox activity of $Ni_{0.31}Co_{0.69}S_2$, good conductivity and high specific surface area of the porous GR framework, the $Ni_{0.31}Co_{0.69}S_2$/GR hydrogels exhibited a remarkable electrocatalytic activity towards glucose oxidation with high sensitivity, low detection limit, wide linear range and low applied potential (Fig. 11(J)). Similarly, Co_3O_4 NPs (Hoa et al., 2016), Prussian blue (Chen et al., 2012b), PdCu NPs (Yuan et al., 2014b), SnO_2 NPs (Li et al., 2015c), and GOx (Wang et al., 2014a) immobilized GR hydrogels showed high analytical performance of target molecules.

2.3.4. Etched GR

In addition to the CVD-grown GR foam, hard-templated porous GR, and GR hydrogels or aerogels, chemical oxidative etching method is also an interesting approach for the synthesis of porous GR because it can introduce defective structure with sp^3 carbon atoms into the basal plane of GR due to redox reaction between the carbon atoms and oxidative reagent. Chemical etching or activation of GR by oxygen plasma (Bai et al., 2010), KOH (Zhu et al., 2011), CO_2 (Yun et al., 2014), H_2O_2 (Palaniselvam et al., 2014), $KMnO_4$ (Fan et al., 2012), copper ions (Wang et al., 2014b), and water steam (Han et al., 2011) can produce pores on the surface of GR, originating from the removal of some sp^2 carbon atoms from the plane. As electrochemical sensors and biosensors, copper ion-etched porous GR showed high analytical performance for small molecules and biomolecules (Wang et al., 2014b). The basal plane of GR was distributed by the redox reaction between the copper ions and sp^2 carbon atoms at high temperature, which induced carbon vacancies or defective sites in the basal plane. The more defective sites of etched porous GR contributed to the high activity of porous GR compared with the pristine GR. Besides these harsh etching reagents, Han et al. reported a slow and more controllable etching route to produce nanoporous GR sheets by hydrothermal steaming at 200 °C (Han et al., 2011). On the basis of their observations, in contrast to nonporous GR annealed at the same temperature, the steamed nanoporous GR-based sensor platform exhibited nearly 2 orders of magnitude increase in the sensitivity and improved recovery time for NO_2 detection. However, due to redox reaction between the carbon atoms and the activation/etching reagents, carbon atoms of GR are consumed for generation of pores in GR, which indicates that the relatively low productivity may make such method unsuitable for large-scale synthesis (Bo et al., 2014).

Table 1 summarizes the analytical performance in terms of the sensitivity, linear range, and limit of detection (LOD) towards the target analytes for the less aggregated GR materials. As discussed above, because of the strong π-π interactions between the GR sheets, aggregation of GR layers usually occurs when GR is immobilized on the electrode surface, leading to single layer GR into quasi-GR consisting of few or multi-layers onto an electrode surface. The GR aggregation significantly limits the performance of GR-based electrochemical sensors or biosensors by the decrease of accessible surface area and active sites. The approaches to alleviate such problems, as noted above, are intercalation of carbon nanomaterials, noncovalent functionalization and covalently

Table 1
Analytical performance of less aggregated GR-based electrochemical sensors or biosensors.

Analyte	Electrode	Sensitivity	Linear range	LOD	Reference
H_2O_2	CNTs/GR	2732.4 μA mM^{-1} cm^{-2}	0.5–5 M	1.3 μM	(Huang et al. 2013)
NADH		204 μA mM^{-1} cm^{-2}	0.02–0.4 mM	0.078 μM	
Tyrosine	CNTs/GR	–	0.9–112 μM	0.09 μM	(Arvand and Gholizadeh, 2013)
Paracetamol			0.9–100 μM	0.2 μM	
DA	PTCA/CNTs/GR/IL	15 μA mM^{-1}	0.03–3800 μM	1.2 nM	(Niu et al. 2013)
Glucose	CuO/carbon nanofiber/GR	912.7 μA mM^{-1} cm^{-2}	1–5300 μM	0.1 μM	(Ye et al. 2013)
Cefepime	Pt/carbon nanosphere/GR	1747.2 μA mM^{-1}	0.008–6.0 μM	0.001 μM	(Shahrokhian et al. 2014)
Glucose	Pt/macroporous carbon/GR	0.45 mA mg^{-1} mM^{-1}	0.1–9.8 mM	40 μM	(Bo and Guo, 2013)
2,4-dinitrotoluene 1,3,5-trinitrophenol	PtPd/CNTs/GR	–	3.5–190 ppb	1 ppb	(Yuan et al., 2014a)
			1–115 ppb	0.52 ppb	
Nitrobenzene			1–155 ppb	0.42 ppb	
Para-nitroaniline			1–115 ppb	0.62 ppb	
H_2O_2	$Ni(OH)_2$/CNTs/GR	717 μA mM^{-1} cm^{-2}	0.01–9.05 mM	4.0 μM	(Gao et al. 2014)
Glucose		2042 μA mM^{-1} cm^{-2}	0.01–1.5 mM	2.7 μM	
glucose	Pt/CNTs/GR	11.06 μA mM^{-1} cm^{-2}	1–7 mM	0.387 mM	(Badhulika et al. 2014)
H_2O_2	PtAu/CNTs/GR	313.4 μA mM^{-1} cm^{-2}	2–8561 μM	0.6 μM	(Lu et al., 2013b)
Glucose	GOx/Au/CNTs/GR	29.72 mA M^{-1} cm^{-2}	5–175 μM	4.8 μM	(Yu et al. 2014b)
Glucose	GOx/ZnO/CNTs/GR	5.36 (± 0.072) μA mM^{-} cm^{-2}	0.01–6.5 mM	4.5 (± 0.08) μM	(Hwa and Subramani, 2014)
UA	Au/PDDA/GR	103.08 μA μM^{-1} cm^{-2}	0.1 μM	0.5–20 μM	(Xue et al. 2011)
Glucose	GR/PFIL/GOx	–	2–14 mM	–	(Shan et al., 2009b)
H_2O_2	Ag/PQ11/GR	–	0.1–40 mM	28 μM	(Liu et al. 2010b)
H_2O_2	Au/PDDA/GR	–	0.5–50 μM	0.22 μM	(Fang et al. 2010)
H_2O_2	HRP/SDBS/GR	220 μA mM^{-1} cm^{-2}	1–2600 μM	0.1 μM	(Zeng et al., 2010)
Glucose	GOx/PDDA/GR	154.9 μA mM^{-1} cm^{-2}	0.02–1.8 mM	8 μM	(Jia et al. 2013)
Nitrophenol	HP-β-CD/GR	–	5×10^{-8}–1×10^{-4} M	10 μM	(Xu et al. 2011a)
Glucose	[IL-GR/(s-GR)]n	0.0718 ± 0.00648 nA μM^{-1}	10 μM–500 μM	3.33 μM	(Gu et al. 2012)
Trinitrotoluene	IL-GR	351.1 μA mg^{-1} L	0.03 – 1.5 ppm	4 ppb	(Guo et al. 2011a)
UA	neutral red/GR	–	0.125–12.25 μM	0.062 μM	(Song et al. 2012)
AA	PTCA/GR	25.64 μA mM^{-1} cm^{-2}	20–420 μM	5.60 μM	(Zhang et al., 2012b)
DA		57.52 μA mM^{-1} cm^{-2}	0.40–374 μM	0.13 μM	
UA		99.27 μA mM^{-1} cm^{-2}	4–544 μM	0.92 μM	
Tryptophan		215.97 μA mM^{-1} cm^{-2}	0.40–138 μM	0.06 μM	
H_2O_2	Pt/GR foam	–	0.167–7.486 μM	0.125 μM	(Cao et al., 2013)
	CNTs/GR foam		20–280 μM	6.54 μM	
	Pt/CNTs/GR foam		0.025–6.3 μM	8.6 nM	
	MnO_2/GR foam		0.38–13.46 μM	0.27 μM	
UA	ZnO NWA/GR foam	–	–	0.5 μM	(Yue et al., 2014)
DA				0.5 μM	
AA				5 μM	
H_2O_2	porous GR	6.20×10^{-4} A M^{-1} cm^{-2}	–	1.94 μM	(Wang et al. 2014b)
NADH		5.12×10^{-3} A M^{-1} cm^{-2}		0.53 μM	
DA	GR foam	619.6 μA mM^{-1} cm^{-2}	25 μM	25 nM	(Liu et al. 2012b)
DNA bases	RGNW	–	0.1 fM–1 μM	9.4 zM	(Akhavan et al. 2012)
DA	GR foam	619.6 μA mM^{-1} cm^{-2}	up to 25 μM	25 nM	(Dong et al., 2012b)
H_2O_2	Ag /GR foam	1094 μA mM^{-1} cm^{-2}	0.03–16.21 mM	14.9 μM	(Zhan et al., 2014b)
Glucose	Mn_3O_4/GR foam	360 μA mM^{-1} cm^{-2}	0.1–8 mM	10 μM	(Si et al. 2013)
UA	Au/GR hydrogel	10.07 μA μM^{-1} cm^{-2}	2–40 μM	0.48 μM	(Du et al., 2014)
Glucose	$NiCo_2O_4$/GR foam	2524 μA mM^{-1} cm^{-2}	0.0005–0.59 mM	0.38 μM	(Wu et al. 2015)
Glucose	$Ni(OH)_2$/GR foam	2650 μA mM^{-1} cm^{-2}	0.001–1.17 mM	0.34 μM	(Zhan et al., 2014a)
AA	CuO/GR foam	2060 μA mM^{-1} cm^{-2}	0.43–200 μM	0.43 μM	(Ma et al. 2014)
H_2 O_2	PtRu/GR foam	1023.1 μA mM^{-1} cm^{-2}	0.005–0.02 mM	0.04 μM	(Kung et al. 2014)
H_2O_2	Pt/porous GR	341.14 μA mM^{-1} cm^{-2}	1–1477 μM	0.50 μM	(Liu et al. 2015a)

functionalization of GR, and structural engineering, where GR is constructed into less aggregated structure such that the electronic and structural properties of GR may be fully utilized. With high dispersion and high surface area for both efficient exposure of active sites or supported NPs and electrolyte-reactant diffusion, the less aggregated GR exhibits remarkable activity towards the target analytes. The high activity can be experimentally observed in the case of CNTs/GR towards the detection of H_2O_2 and NADH in which CNTs/GR showed substantial improvements in electrochemical reactivity and LOD relative to those obtained from GR and CNTs-modified electrodes (Huang et al., 2013). Furthermore, the electrochemical activity or selectivity of CNTs can be improved by incorporation of NPs (Hwa and Subramani, 2014; Yu et al., 2014b; Yuan et al., 2014a), or enzymes (Mani et al., 2013a; Sun et al., 2013). Similar conclusions are arrived at tyrosine (Arvand and Gholizadeh, 2013), tetrabromobisphenol A (Zhang et al., 2015b), glucose (Mani et al., 2013a), nitro aromatic compound (Yuan et al., 2014a), and DA (Niu et al., 2013). Besides intercalation of carbon nanomaterials, surface functionalization of GR is similarly found to be attractive for alleviation of GR aggregation. Noncovalent or covalent functionalization of GR with polymers, polyelectrolytes, or organic molecules also effectively prevents the aggregation of GR layers. As electrochemical sensors or biosensors, it is shown to give rise to an improved linear range and limit of detection towards some analytes, such as angiogenin (Chen et al., 2014), glucose (Gu et al., 2012), H_2O_2 (Zeng et al., 2010), and cancer cells (Feng et al., 2011). Notably, impressive analytical performance of surface functionalized GR suggested noncovalently or covalently functionalized GR with high dispersion maximally expose the active sites or supported NPs or biomolecules towards the analytes, thereby affording high activity. Additionally, various structural engineering strategies have been applied to proliferate the

Table 2
Comparison of analytical performance of less aggregated GR and pristine GR-based sensors.

Analyte	Electrode	Sensitivity	Linear range	LOD	Reference
H_2O_2	Pt/GR	10 μA mM^{-1}	2–712 μM	0.5 μM	(Xu et al. 2011b)
H_2O_2	GR	–	0.05–1500 μM	0.05	(Zhou et al., 2009)
H_2O_2	Au NPs/POM/GR	58.87 μA mM^{-1} cm^{-2}	5–18000 μM	1.54 μM	(Liu et al. 2012a)
H_2O_2	Pt/GR	–	1–500 μM	0.08 μM	(Guo et al. 2010a)
H_2O_2	Pt/porous GR	341.14 μA mM^{-1} cm^{-2}	1–1477 μM	0.05 μM	(Liu et al. 2015a)
H_2O_2	CNTs/GR	2732.4 μA mM^{-1} cm^{-2}	500–5000 μM	1.3 μM	(Huang et al. 2013)
H_2O_2	Au/PDDA/GR	–	0.5–500 μM	0.44 μM	(Fang et al. 2010)
H_2O_2	PtAu NPs/CNTs/GR	313.4 μA mM^{-1} cm^{-2}	2–8561 μM	0.6 μM	(Lu et al., 2013b)
H_2O_2	Hb/Au/GR	47.1 μA mM^{-1} cm^{-2}	2–935 μM	0.35 μM	(Zhang et al., 2014)
H_2O_2	HRP/Au/GR	–	5–5130 μM	1.7 M	(Zhou et al., 2010)
H_2O_2	HRP/SDBS/GR	220 μA mM^{-1} cm^{-2}	1–260 μM	0.1 μM	(Zeng et al., 2010)
H_2O_2	Pt/CNTs/PGR		0.025–6.3 μM	0.0086 μM	(Cao et al., 2013)
Glucose	GOx/GR	20.21 μA mM^{-1} cm^{-2}	0.01–10 mM	2.0 μM	(Zhou et al., 2009)
Glucose	GOx/GR	37.93 μA mM^{-1} cm^{-2}	0.08–12 mM	20 μM	(Kang et al. 2009)
Glucose	GOx/Pt/GR	–	0.01–50 mM	0.3 μM	(Claussen et al., 2012)
Glucose	GOx/Pt/GR	–	Up to 5 mM	0.6 μM	(Wu et al. 2009)
Glucose	GR/PFIL/GOx	–	2–14 mM	–	(Shan et al., 2009b)
Glucose	CuO/GR	1360 μA mM^{-1} cm^{-2}	0.002–4 mM	0.7 μM	(Luo et al. 2012)
Glucose	$Ni(OH)_2$/GR	11.43 μA mM^{-1} cm^{-2}	0.002–3.1 mM	0.6 μM	(Zhang et al., 2011c)
Glucose	$Ni(OH)_2$/CNTs/GR	2042 μA mM^{-1} cm^{-2}	0.01–1.5 mM	2.7 μM	(Gao et al. 2014)
Glucose	$Ni_{0.31}Co_{0.69}S_2$/GR	1753 μA mM^{-1} cm^{-2}	0.001–5 mM	0.078 μM	(Li et al. 2015a)
Glucose	Co_3O_4/GR foam	3390 μA mM^{-1} cm^{-2}	Up to 80 μM	25 nM	(Dong et al., 2012a)
Glucose	$Ni(OH)_2$/GR foam	2650 μA mM^{-1} cm^{-2}	0.001–1.17 mM	0.34 μM	(Zhan et al., 2014a)
Glucose	$NiCo_2O_4$/GR foam	2524 μA mM^{-1} cm^{-2}	0.0005–0.59 mM	0.38 μM	(Wu et al. 2015)
Glucose	$Cu(OH)_2$/foam	3360 μA mM^{-1} cm^{-2}	0.0012–6 mM	1.2 μM	(Shackery et al. 2016)

exposed edge sites of GR for enhanced performance. The role of nanostructures in improving analytical performance was clearly exemplified by the high activity of RGNW (Akhavan et al., 2012). By construction of GR into nanowall structure, the more active edge sites are exposed to G, A, T, and C, exhibiting high current towards the G, A, T, and C compared to RGNS, GONW graphite, and GC electrodes. Building on the same principles, another important study comparing the detection of DA at GR foam and GC also emphasized the promotion effect of nanostructure (Dong et al., 2012b). The role of GR nanostructures for improving the electrocatalytic activity was further demonstrated by the high analytical performance of GR hydrogels or aerogels (Cai et al., 2016). The increased distance between layers and high surface area of structural engineered GR ensure the efficient exposure more active sites and fast mass transfer, which consequently leads to excellent activity. The structural properties of GR nanostructures satisfy the requirements of an ideal support, which facilitate the exposure of supported NPs or biomolecules and increase the utilization efficiency of supported inorganic nanomaterials, antibodies, or enzymes. For example, the Co_3O_4 nanowires/porous GR foam showed high performance as an enzyme-free ultrasensitive sensor of glucose because of the synergistic interaction between the Co_3O_4 nanowires and porous GR foam (Dong et al., 2012a). In the same manner, ZnO NWA supported on the porous GR foam also showed high performance for AA, UA and DA, exhibiting a detection limit of 1 nM for UA and DA (Yue et al., 2014). In summary, observation of the analytical performance in Table 1 indicates that the less aggregated GR appears to exhibit improvements over that of pristine GR. This improved performance corresponds well with the unique structural properties of less aggregated GR, likely due to the large surface area and high dispersion of less aggregated GR.

In Table 2, glucose and H_2O_2 are selected as typical analytes to compare the analytical performance between the less aggregated GR and pristine GR. Because of the different loading amount, preparation method, operation condition, and detection method, cross-laboratory comparison of analytical performance is difficult. However, some general trends can be found from the comparison in Table 2. To emphasize the advantages of using less aggregated GR for the construction of electrochemical sensors or biosensors, some typical sensors for glucose and H_2O_2 are listed in Table 2. In the case of H_2O_2, high sensitivities are observed at Pt/porous GR (Liu et al., 2015a), CNTs/GR (Huang et al., 2013), PtAu NPs/CNTs/GR (Lu et al., 2013b) compared to Au NPs/POM/GR (Liu et al., 2012a). This observation reflects the superior performance of less aggregated GR over pristine GR as an electrode material. Similar behavior is also observed for enzyme-based H_2O_2 biosensor with a sensitivity of 220 μA mM^{-1} cm^{-2} and LOD of 0.1 μM at the HRP/SDBS/GR (Zeng et al., 2010), compared to sensitivity of 47.1 μA mM^{-1} cm^{-2} and LOD of 0.35 μM at Hb/Au/GR (Zhang et al., 2014). Due to its high surface area, high dispersion, or abundant pores, the less aggregated GR-based sensors or biosensors exhibit high analytical performance for H_2O_2 as compared to pristine GR. The enzyme-based H_2O_2 biosensors generate high activity and selectivity. However, due to the low stability and high cost of enzymes, the wide utilization of enzyme-based H_2O_2 biosensors may be hindered. The replacement of enzyme-based H_2O_2 biosensors with inexpensive inorganic nanomaterials is a desired way to overcome the low stability and high cost of enzymes. Using glucose as a comparison between less aggregated GR and pristine GR is also presented in Table 2. Compared to LOD of 20 μM at GOx/GR (Kang et al., 2009), a low LOD of 4.8 μM is obtained at GOx/Au/CNTs/GR (Yu et al., 2014b), indicating the better analytical performance of GOx/Au/CNTs/GR. Compared with pristine GR-based nonenzymatic glucose sensors (CuO/GR (Luo et al., 2012) and Ni$(OH)_2$/GR (Zhang et al., 2011c), less aggregated GR-based nonenzymatic glucose sensors also show high activity, such as $Ni(OH)_2$/CNTs/GR (Gao et al., 2014), $Ni_{0.31}Co_{0.69}S_2$/GR (Li et al., 2015a), Co_3O_4/porous GR foam (Dong et al., 2012a), $Ni(OH)_2$/porous GR foam (Zhan et al., 2014a), $NiCo_2O_4$/porous GR foam (Wu et al., 2015), $Cu(OH)_2$/porous GR (Shackery et al., 2016). From the electrochemical data in Table 2, nonenzymatic glucose sensors showed high sensitivity than GOx-based biosensors. However, the alkaline electrolyte is required to realize the direct oxidation of glucose, which may limit the practical applications of nonenzymatic glucose sensors. As evident from the data in Table 2, generally, the less aggregated GR-based sensors or biosensors show higher sensitivity than pristine GR. The high sensitivity observed at less aggregated GR-based sensors or biosensors is predominantly dictated by the structural properties of less aggregated GR, such as high dispersion, fast mass transfer, large surface area, and efficient

exposure of supported NPs or biomolecules.

3. Outlook and conclusion

Since 2008, GR has been widely used in the design and construction of electrochemical sensors and biosensors to improve the performance of those devices. To alleviate the irreversible aggregation of GR layers and increase the analytical performance, less aggregated GR with large surface area, high-density active sites and porous structure has been applied to construct various attractive electrochemical sensors and biosensors. A variety of methods including intercalation of carbon materials, surface modification, and structural engineering are developed for preparing less aggregated GR materials. The less aggregated GR not only enables high density of active sites but also provides large surface area for loading inorganic NPs, organic or biological molecules. Although considerable progress has been made in the development of less aggregated GR-based electrochemical sensors and biosensors, many challenges and exciting opportunities still remain in such field.

(1) What are the exact electrocatalytic mechanisms of GR? By surface or structural engineering the synthesis of GR to yield less aggregate GR with a high surface area and porous morphology, the edge sites of GR are fully exposed, enhancing its electrocatalytic performance. Insights from Banks confirmed that edge plane sites/defects are the predominant origin of electrochemical activity of GR (Brownson et al. 2012). By comparing the electrocatalytic activities between GR and anodized GR, Lim et al. gave the same opinion that the enhanced catalytic activity of anodized GR compared to pristine GR originated from the more edge plane sites/defects (Lim et al. 2010). Shi's group similarly demonstrated that GR edge possesses much stronger electrocatalytic activity than GR basal plane (Yuan et al., 2013). However, in contrast, Pumera et al. argued that the metallic impurities or residues were the active sites for GR's electrochemistry activity (Ambrosi et al., 2012a, 2012b; Chee and Pumera, 2012; Wang et al., 2015b; Wong et al., 2013). They believed that graphite and CNTs as precursors for GR preparation contain a large amount of metallic impurities that persist in the samples of GO after the oxidative treatment and chemically reduced GR after the chemical reduction. These impurities heavily influenced the electrochemical behavior of the resulting GR material. In addition, by comparing the electrochemical activities between GR and base-treated GR, Zhu et al. revealed that the carbonaceous oxidative debris resided in GR was responsible for the electrochemical activity of GR (Li et al. 2015d; Li et al. 2012a; Yang et al. 2013, 2014). Up to now, the exact nature of the active sites in GR-based sensors and biosensors still remains controversial. Therefore, the real electrocatalytic mechanisms of GR are still unclear and further investigations are still required in the future.

(2) The surface-functionalized (noncovalently or covalently functionalized) GR nanomaterials exhibit high stability in solvent. This is because that the charged groups on surface-functionalized GR surface would prevent the aggregation of GR sheets induced by the electrostatic repulsion in solution. However, those high-stable surface-functionalized GR nanomaterials will still become the irreversibly precipitated agglomerates when they are dry on electrode surface. Thus, how to alleviate the aggregation of dry-state surface-functionalized GR on electrode surface still needs more investigation.

(3) Although some literatures indicated that less aggregated GR-based sensors and biosensors exhibited prominent ability in real simple detection, currently, most of the electrochemical sensors and biosensors are still limited for lab demonstrations, suggesting they are far away from the commercial markets. Therefore, further studies are required to accelerate the commercialization of sensors and biosensors based on less aggregated GR with high safety and health, high competitiveness to the current technologies.

We believe that less aggregated GR-based electrochemical sensors and biosensors with their remarkable and unique analytical performances will continue to attract increasing research interest and lead to new opportunities in diverse research fields.

Acknowledgments

Financial support from National Natural Science Foundation of China (21405011) is highly appreciated. M. Z. is grateful to the financial support from Northeast Normal University startup funds, Jilin Provincial Department of Education, and the Recruitment Program of Global Youth Experts.

References

Akhavan, O., Ghaderi, E., Rahighi, R., 2012. ACS Nano 6 (4), 2904–2916.
Ambrosi, A., Chee, S.Y., Khezri, B., Webster, R.D., Sofer, Z., Pumera, M., 2012a. Angew. Chem. Int. Ed. 51 (2), 500–503.
Ambrosi, A., Chua, C.K., Khezri, B., Sofer, Z., Webster, R.D., Pumera, M., 2012b. Proc. Nat. Acad. Sci. U. S. A. 109 (32), 12899–12904.
Antiochia, R., Gorton, L., 2014. Sens. Actuators, B 195, 287–293.
Arvand, M., Gholizadeh, T.M., 2013. Colloids Surf. B 103, 84–93.
Avouris, P., Dimitrakopoulos, C., 2012. Mater. Today 15 (3), 86–97.
Badhulika, S., Paul, R.K., Rajesh, Terse, T., Mulchandani, A., 2014. Electroanalysis 26 (1), 103–108.
Bai, J., Zhong, X., Jiang, S., Huang, Y., Duan, X., 2010. Nat. Nanotechnol. 5 (3), 190–194.
Baptista, F.R., Belhout, S.A., Giordani, S., Quinn, S.J., 2015. Chem. Soc. Rev. 44 (13), 4433–4453.
Bo, X., Guo, L., 2013. Electrochim. Acta 90, 283–290.
Bo, X., Han, C., Zhang, Y., Guo, L., 2014. ACS Appl. Mater. Interfaces 6 (4), 3023–3030.
Bo, X., Li, M., Han, C., Guo, L., 2013. Electrochim. Acta 114, 582–589.
Brownson, D.A.C., Figueiredo-Filho, L.C.S., Ji, X., Gómez-Mingot, M., Iniesta, J., Fatibello-Filho, O., Kampouris, D.K., Banks, C.E., 2013. J. Mater. Chem. A 1 (19), 5962.
Brownson, D.A.C., Figueiredo-Filho, L.C.S., Riehl, B.L., Riehl, B.D., Gomez-Mingot, M., Iniesta, J., Fatibello-Filho, O., Banks, C.E., 2016. J. Mater. Chem. A 4 (7), 2617–2629.
Brownson, D.A.C., Kampouris, D.K., Banks, C.E., 2012. Chem. Soc. Rev. 41 (21), 6944–6976.
Byrne, M.T., Gun'ko, Y.K., 2010. Adv. Mater. 22 (15), 1672–1688.
Cai, M., Thorpe, D., Adamson, D.H., Schniepp, H.C., 2012. J. Mater. Chem. 22 (48), 24992–25002.
Cai, Z.-X., Song, X.-H., Chen, Y.-Y., Wang, Y.-R., Chen, X., 2016. Sens. Actuators B 222, 567–573.
Cao, X., Yin, Z., Zhang, H., 2014. Energy Environ. Sci. 7 (6), 1850–1865.
Cao, X., Zeng, Z., Shi, W., Yep, P., Yan, Q., Zhang, H., 2013. Small 9 (9–10), 1703–1707.
Carbone, M., Gorton, L., Antiochia, R., 2015. Electroanalysis 27 (1), 16–31.
Chabot, V., Higgins, D., Yu, A., Xiao, X., Chen, Z., Zhang, J., 2014. Energy Environ. Sci. 7 (5), 1564–1596.
Chee, S.Y., Pumera, M., 2012. Analyst 137 (9), 2039–2041.
Chen, D., Feng, H., Li, J., 2012a. Chem. Rev. 112 (11), 6027–6053.
Chen, L., Wang, X., Zhang, X., Zhang, H., 2012b. J. Mater. Chem. 22 (41), 22090–22096.
Chen, X., Zhu, J., Xi, Q., Yang, W., 2012c. Sens. Actuators B 161 (1), 648–654.
Chen, Z., Ren, W., Gao, L., Liu, B., Pei, S., Cheng, H.-M., 2011. Nat. Mater. 10 (6), 424–428.
Chen, Z., Zhang, C., Li, X., Ma, H., Wan, C., Li, K., Lin, Y., 2014. Biosens. Bioelectron. 65C, 232–237.
Chhowalla, M., Liu, Z., Zhang, H., 2015. Chem. Soc. Rev. 44 (9), 2584–2586.
Chia, X., Eng, A.Y.S., Ambrosi, A., Tan, S.M., Pumera, M., 2015. Chem. Rev. 115 (21), 11941–11966.
Choi, B.G., Yang, M., Hong, W.H., Choi, J.W., Huh, Y.S., 2012. ACS Nano 6 (5), 4020–4028.
Claussen, J.C., Kumar, A., Jaroch, D.B., Khawaja, M.H., Hibbard, A.B., Porterfield, D.M., Fisher, T.S., 2012. Adv. Funct. Mater. 22 (16), 3399–3405.
da Silva, H., Pacheco, J.G., Magalhaes, J.M., Viswanathan, S., Delerue-Matos, C., 2014. Biosens. Bioelectron. 52, 56–61.
Dai, L., 2012. Acc. Chem. Res. 46 (1), 31–42.

Dong, X.-C., Xu, H., Wang, X.-W., Huang, Y.-X., Chan-Park, M.B., Zhang, H., Wang, L.-H., Huang, W., Chen, P., 2012a. ACS Nano 6 (4), 3206–3213.
Dong, X., Cao, Y., Wang, J., Chan-Park, M.B., Wang, L., Huang, W., Chen, P., 2012a. RSC Adv. 2 (10), 4364–4369.
Dong, X., Wang, X., Wang, L., Song, H., Zhang, H., Huang, W., Chen, P., 2012b. ACS Appl. Mater. Interfaces 4 (6), 3129–3133.
Dreyer, D.R., Park, S., Bielawski, C.W., Ruoff, R.S., 2010. Chem. Soc. Rev. 39 (1), 228–240.
Du, C., Yao, Z., Chen, Y., Bai, H., Li, L., 2014. RSC Adv. 4 (18), 9133–9138.
Du, F., Yu, D., Dai, L., Ganguli, S., Varshney, V., Roy, A.K., 2011. Chem. Mater. 23 (21), 4810–4816.
Dubertret, B., Heine, T., Terrones, M., 2015. Acc. Chem. Res. 48 (1), 1–2.
Edwards, R.S., Coleman, K.S., 2013. Nanoscale 5 (1), 38–51.
Fan, Z., Zhao, Q., Li, T., Yan, J., Ren, Y., Feng, J., Wei, T., 2012. Carbon 50 (4), 1699–1703.
Fang, Y., Guo, S., Zhu, C., Zhai, Y., Wang, E., 2010. Langmuir 26 (13), 11277–11282.
Favero, G., Fusco, G., Mazzei, F., Tasca, F., Antiochia, R., 2015. Nanomaterials 5 (4), 1995–2006.
Feng, L., Chen, Y., Ren, J., Qu, X., 2011. Biomaterials 32 (11), 2930–2937.
Feng, L., Liu, Z., 2011. Nanomedicine 6 (2), 317–324.
Feng, Q., Duan, K., Ye, X., Lu, D., Du, Y., Wang, C., 2014. Sens. Actuators B 192, 1–8.
Feng, Q., Liu, K., Fu, J., Zhang, Y., Zheng, Z., Wang, C., Du, Y., Ye, W., 2012. Electrochim. Acta 60, 304–308.
Figueiredo-Filho, L.C.S., Brownson, D.A.C., Fatibello-Filho, O., Banks, C.E., 2014. Electroanalysis 26 (1), 93–102.
Fu, S., Fan, G., Yang, L., Li, F., 2015. Electrochim. Acta 152, 146–154.
Gao, H., Duan, H., 2015. Biosens. Bioelectron. 65, 404–419.
Gao, W., Tjiu, W.W., Wei, J., Liu, T., 2014. Talanta 120, 484–490.
Georgakilas, V., Otyepka, M., Bourlinos, A.B., Chandra, V., Kim, N., Kemp, K.C., Hobza, P., Zboril, R., Kim, K.S., 2012. Chem. Rev. 112 (11), 6156–6214.
Gong, J., Miao, X., Zhou, T., Zhang, L., 2011. Talanta 85 (3), 1344–1349.
Gu, H., Yu, Y., Liu, X., Ni, B., Zhou, T., Shi, G., 2012. Biosens. Bioelectron. 32 (1), 118–126.
Guo, C.X., Ng, S.R., Khoo, S.Y., Zheng, X., Chen, P., Li, C.M., 2012. ACS Nano 6 (8), 6944–6951.
Guo, S., Dong, S., 2011. Chem. Soc. Rev. 40 (5), 2644–2672.
Guo, S., Wen, D., Zhai, Y., Dong, S., Wang, E., 2010a. ACS Nano 4 (7), 3959–3968.
Guo, S., Wen, D., Zhai, Y., Dong, S., Wang, E., 2011a. Biosens. Bioelectron. 26 (8), 3475–3481.
Guo, Y., Guo, S., Ren, J., Zhai, Y., Dong, S., Wang, E., 2010b. ACS Nano 4 (7), 4001–4010.
Guo, Y., Li, J., Dong, S., 2011b. Sens. Actuators B 160 (1), 295–300.
Guo, Y., Xu, K., Wu, C., Zhao, J., Xie, Y., 2015. Chem. Soc. Rev. 44, 637–646.
Han, S., Wu, D., Li, S., Zhang, F., Feng, X., 2014. Adv. Mater. 26 (6), 849–864.
Han, T.H., Huang, Y.K., Tan, A.T., Dravid, V.P., Huang, J., 2011. J. Am. Chem. Soc. 133 (39), 15264–15267.
Harada, A., 2001. Acc. Chem. Res. 34 (6), 456–464.
He, W., Sun, Y., Xi, J., Abdurhman, A.A.M., Ren, J., Duan, H., 2016. Anal. Chim. Acta 903, 61–68.
Ho, T.D., Zhang, C., Hantao, L.W., Anderson, J.L., 2014. Anal. Chem. 86 (1), 262–285.
Hoa, L.T., Chung, J.S., Hur, S.H., 2016. Sens. Actuators B 223, 76–82.
Hou, S., Kasner, M.L., Su, S., Patel, K., Cuellari, R., 2010. J. Phys. Chem. C. 114 (35), 14915–14921.
Hu, F.X., Xie, J.L., Bao, S.J., Yu, L., Li, C.M., 2015. Biosens. Bioelectron. 70, 310–317.
Hu, Y., Wang, K., Zhang, Q., Li, F., Wu, T., Niu, L., 2012. Biomaterials 33 (4), 1097–1106.
Huan, J., Liu, Q., Fei, A., Qian, J., Dong, X., Qiu, B., Mao, H., Wang, K., 2015. Biosens. Bioelectron. 73, 221–227.
Huang, T.Y., Huang, J.H., Wei, H.Y., Ho, K.C., Chu, C.W., 2013. Biosens. Bioelectron. 43, 173–179.
Huang, X., Qi, X., Boey, F., Zhang, H., 2012a. Chem. Soc. Rev. 41 (2), 666–686.
Huang, X., Qian, K., Yang, J., Zhang, J., Li, L., Yu, C., Zhao, D., 2012b. Adv. Mater. 24 (32), 4419–4423.
Hummers Jr, W.S., Offeman, R.E., 1958. J. Am. Chem. Soc. 80 (6), 1339.
Hwa, K.Y., Subramani, B., 2014. Biosens. Bioelectron. 62, 127–133.
Jia, L., Liu, J., Wang, H., 2013. Electrochim. Acta 111, 411–418.
Ju, J., Chen, W., 2015. Anal. Chem. 87 (3), 1903–1910.
Juanjuan, Z., Ruiyi, L., Zaijun, L., Junkang, L., Zhiguo, G., Guangli, W., 2014. Nanoscale 6 (10), 5458–5466.
Kang, X., Wang, J., Wu, H., Aksay, I.A., Liu, J., Lin, Y., 2009. Biosens. Bioelectron. 25 (4), 901–905.
Karousis, N., Tagmatarchis, N., Tasis, D., 2010. Chem. Rev. 110 (9), 5366–5397.
Kochmann, S., Hirsch, T., Wolfbeis, O.S., 2012. Trac. Trends Anal. Chem. 39, 87–113.
Komori, K., Terse-Thakoor, T., Mulchandani, A., 2015. ACS Appl. Mater. Interfaces 7 (6), 3647–3654.
Kuila, T., Bose, S., Khanra, P., Mishra, A.K., Kim, N.H., Lee, J.H., 2011. Biosens. Bioelectron. 26 (12), 4637–4648.
Kumar, S., Ahlawat, W., Kumar, R., Dilbaghi, N., 2015. Biosens. Bioelectron. 70, 498–503.
Kung, C.C., Lin, P.Y., Buse, F.J., Xue, Y., Yu, X., Dai, L., Liu, C.C., 2014. Biosens. Bioelectron. 52, 1–7.
Lawal, A.T., 2015. Talanta 131, 424–443.
Leng, C., Wu, J., Xu, Q., Lai, G., Ju, H., Yan, F., 2011. Biosens. Bioelectron. 27 (1), 71–76.
Li, C., Shi, G., 2012. Nanoscale 4 (18), 5549–5563.
Li, G., Huo, H., Xu, C., 2015a. J. Mater. Chem. A 3 (9), 4922–4930.
Li, H., Wang, Y., Ye, D., Luo, J., Su, B., Zhang, S., Kong, J., 2014. Talanta 127, 255–261.
Li, J., Jiang, J., Feng, H., Xu, Z., Tang, S., Deng, P., Qian, D., 2016. RSC Adv. 6 (37), 31565–31573.
Li, J., Xie, J., Gao, L., Li, C.M., 2015b. ACS Appl. Mater. Interfaces 7 (4), 2726–2734.
Li, L., He, S., Liu, M., Zhang, C., Chen, W., 2015c. Anal. Chem. 87 (3), 1638–1645.
Li, S., Purdy, W.C., 1992. Chem. Rev. 92 (6), 1457–1470.
Li, X., Ma, D., Zhu, L., 2015d. Chem. Eur. J. 21 (48), 17239–17244.
Li, X., Yang, X., Jia, L., Ma, X., Zhu, L., 2012a. Electrochem. Commun. 23 (1), 94–97.
Li, Y., Li, Y., Zhu, E., McLouth, T., Chiu, C.-Y., Huang, X., Huang, Y., 2012b. J. Am. Chem. Soc. 134 (30), 12326–12329.
Lim, C.X., Hoh, H.Y., Ang, P.K., Loh, K.P., 2010. Anal. Chem. 82 (17), 7387–7393.
Liu, G.T., Chen, H.F., Lin, G.M., Ye, P.P., Wang, X.P., Jiao, Y.Z., Guo, X.Y., Wen, Y., Yang, H.F., 2014a. Biosens. Bioelectron. 56, 26–32.
Liu, H., Gao, J., Xue, M., Zhu, N., Zhang, M., Cao, T., 2009. Langmuir 25 (20), 12006–12010.
Liu, J., Bo, X., Zhao, Z., Guo, L., 2015a. Biosens. Bioelectron. 74, 71–77.
Liu, J., Wang, J., Wang, T., Li, D., Xi, F., Wang, J., Wang, E., 2014a. Biosens. Bioelectron. 65, 281–286.
Liu, J., Wang, X., Wang, T., Li, D., Xi, F., Wang, J., Wang, E., 2014b. ACS Appl. Mater. Interfaces 6 (22), 19997–20002.
Liu, K., Zhang, J., Yang, G., Wang, C., Zhu, J.-J., 2010a. Electrochem. Commun. 12 (3), 402–405.
Liu, L., Zhai, J., Zhu, C., Gao, Y., Wang, Y., Han, Y., Dong, S., 2015b. Biosens. Bioelectron. 63, 483–489.
Liu, M., Zhang, R., Chen, W., 2014d. Chem. Rev. 114 (10), 5117–5160.
Liu, R., Li, S., Yu, X., Zhang, G., Zhang, S., Yao, J., Keita, B., Nadjo, L., Zhi, L., 2012a. Small 8 (9), 1398–1406.
Liu, S., Tian, J., Wang, L., Li, H., Zhang, Y., Sun, X., 2010b. Macromolecules 43 (23), 10078–10083.
Liu, S., Tian, J., Wang, L., Sun, X., 2011. Carbon 49 (10), 3158–3164.
Liu, W., Zhang, J., Li, C., Tang, L., Zhang, Z., Yang, M., 2013. Talanta 104, 204–211.
Liu, Y., Dong, X., Chen, P., 2012b. Chem. Soc. Rev. 41 (6), 2283–2307.
Loryuenyong, V., Totepvimarn, K., Eimburanapravat, P., Boonchompoo, W., Buasri, A., 2013. Adv. Mater. Sci. Eng. 2013, 923403.
Lu, D., Lin, S., Wang, L., Li, T., Wang, C., Zhang, Y., 2013a. J. Solid State Electrochem. 18 (1), 269–278.
Lu, D., Zhang, Y., Lin, S., Wang, L., Wang, C., 2013b. Talanta 112, 111–116.
Lu, D., Zhang, Y., Wang, L., Lin, S., Wang, C., Chen, X., 2012. Talanta 88, 181–186.
Luo, L., Zhu, L., Wang, Z., 2012. Bioelectrochemistry 88, 156–163.
Ma, Y., Zhao, M., Cai, B., Wang, W., Ye, Z., Huang, J., 2014. Biosens. Bioelectron. 59, 384–388.
Mani, V., Devadas, B., Chen, S.M., 2013a. Biosens. Bioelectron. 41, 309–315.
Mani, V., Wu, T.-Y., Chen, S.-M., 2013b. J. Solid State Electrochem. 18 (4), 1015–1023.
Mao, S., Lu, G., Chen, J., 2015. Nanoscale 7 (16), 6924–6943.
Mao, S., Yu, K., Chang, J., Steeber, D.A., Ocola, L.E., Chen, J., 2013. Sci. Rep. 3, 1696.
Mas-Balleste, R., Gomez-Navarro, C., Gomez-Herrero, J., Zamora, F., 2011. Nanoscale 3 (1), 20–30.
Mattevi, C., Kim, H., Chhowalla, M., 2011. J. Mater. Chem. 21 (10), 3324–3334.
Meng, Y., Wang, K., Zhang, Y., Wei, Z., 2013. Adv. Mater. 25 (48), 6985–6990.
Nardecchia, S., Carriazo, D., Ferrer, M.L., Gutierrez, M.C., del Monte, F., 2013. Chem. Soc. Rev. 42 (2), 794–830.
Nayak, P., Anbarasan, B., Ramaprabhu, S., 2013. J. Phys. Chem. C. 117 (25), 13202–13209.
Niu, X., Yang, W., Guo, H., Ren, J., Gao, J., 2013. Biosens. Bioelectron. 41, 225–231.
Novoselov, K.S., Geim, A.K., Morozov, S.V., Jiang, D., Zhang, Y., Dubonos, S.V., Grigorieva, I.V., Firsov, A.A., 2004. Science 306 (5696), 666–669.
Palaniselvam, T., Valappil, M.O., Illathvalappil, R., Kurungot, S., 2014. Energy Environ. Sci. 7 (3), 1059–1067.
Patil, U., Lee, S.C., Kulkarni, S., Sohn, J.S., Nam, M.S., Han, S., Jun, S.C., 2015. Nanoscale 7 (16), 6999–7021.
Ping, J., Zhou, Y., Wu, Y., Papper, V., Boujday, S., Marks, R.S., Steele, T.W.J., 2015. Biosens. Bioelectron. 64, 373–385.
Prasannakumar, S., Manjunatha, R., Nethravathi, C., Suresh, G.S., Rajamathi, M., Venkatesha, T.V., 2012. J. Solid State Electrochem. 16 (10), 3189–3199.
Pumera, M., 2009. Chem. Rec. 9 (4), 211–223.
Pumera, M., Ambrosi, A., Bonanni, A., Chng, E.L.K., Poh, H.L., 2010. Trac., Trends Anal. Chem. 29 (9), 954–965.
Qiu, J.D., Shi, L., Liang, R.P., Wang, G.C., Xia, X.H., 2012. Chem. Eur. J. 18 (25), 7950–7959.
Qiu, X., Lu, L., Leng, J., Yu, Y., Wang, W., Jiang, M., Bai, L., 2016. Food Chem. 190, 889–895.
Rotariu, L., Istrate, O.-M., Bala, C., 2014. Sens. Actuators, B 191, 491–497.
Ruecha, N., Rangkupan, R., Rodthongkum, N., Chailapakul, O., 2014. Biosens. Bioelectron. 52, 13–19.
Sajid, M., Nazal, M.K., Mansha, M., Alsharaa, A., Jillani, S.M.S., Basheer, C., 2016. Trac. Trends Anal. Chem. 76, 15–29.
Shackery, I., Patil, U., Pezeshki, A., Shinde, N.M., Kang, S., Im, S., Jun, S.C., 2016. Electrochim. Acta 191, 954–961.
Shahriary, L., Ghourchian, H., Athawale, A.A., 2014. J. Nanotechnol. 2014, 1–10.
Shahrokhian, S., Hosseini-Nassab, N., Ghalkhani, M., 2014. RSC Adv. 4 (15), 7786–7794.
Shan, C., Yang, H., Han, D., Zhang, Q., Ivaska, A., Niu, L., 2009a. Langmuir 25 (20), 12030–12033.
Shan, C., Yang, H., Han, D., Zhang, Q., Ivaska, A., Niu, L., 2010. Biosens. Bioelectron. 25 (5), 1070–1074.
Shan, C., Yang, H., Song, J., Han, D., Ivaska, A., Niu, L., 2009b. Anal. Chem. 81 (6), 2378–2382.

Shang, N.G., Papakonstantinou, P., McMullan, M., Chu, M., Stamboulis, A., Potenza, A., Dhesi, S.S., Marchetto, H., 2008. Adv. Funct. Mater. 18 (21), 3506–3514.
Shao, Y., Wang, J., Wu, H., Liu, J., Aksay, I.A., Lin, Y., 2010. Electroanalysis 22 (10), 1027–1036.
Sheng, Q., Wang, M., Zheng, J., 2011. Sens. Actuators B 160 (1), 1070–1077.
Sheng, Z.H., Zheng, X.Q., Xu, J.Y., Bao, W.J., Wang, F.B., Xia, X.H., 2012. Biosens. Bioelectron. 34 (1), 125–131.
Shiddiky, M.J.A., Torriero, A.A.J., 2011. Biosens. Bioelectron. 26 (5), 1775–1787.
Si, P., Dong, X.-C., Chen, P., Kim, D.-H., 2013. J. Mater. Chem. B 1 (1), 110–115.
Si, Y., Samulski, E.T., 2008. Chem. Mater. 20 (21), 6792–6797.
Song, J., Qiao, J., Shuang, S., Guo, Y., Dong, C., 2012. J. Mater. Chem. 22 (2), 602–608.
Song, Y., Luo, Y., Zhu, C., Li, H., Du, D., Lin, Y., 2016. Biosens. Bioelectron. 76, 195–212.
Su, B., Tang, D., Li, Q., Tang, J., Chen, G., 2011. Anal. Chim. Acta 692 (1–2), 116–124.
Sudeep, P.M., Narayanan, T.N., Ganesan, A., Shaijumon, M.M., Yang, H., Ozden, S., Patra, P.K., Pasquali, M., Vajtai, R., Ganguli, S., 2013. ACS Nano 7 (8), 7034–7040.
Sun, W., Cao, L., Deng, Y., Gong, S., Shi, F., Li, G., Sun, Z., 2013. Anal. Chim. Acta 781, 41–47.
Teymourian, H., Salimi, A., Khezrian, S., 2013. Biosens. Bioelectron. 49, 1–8.
Tran, H.V., Piro, B., Reisberg, S., Huy Nguyen, L., Dung Nguyen, T., Duc, H.T., Pham, M. C., 2014. Biosens. Bioelectron. 62, 25–30.
Valentini, F., Romanazzo, D., Carbone, M., Palleschi, G., 2012. Electroanalysis 24 (4), 872–881.
Vashist, S.K., Luong, J.H.T., 2015. Carbon 84, 519–550.
Wajid, A.S., Das, S., Irin, F., Ahmed, H.S.T., Shelburne, J.L., Parviz, D., Fullerton, R.J., Jankowski, A.F., Hedden, R.C., Green, M.J., 2012. Carbon 50 (2), 526–534.
Wang, B., Yan, S., Shi, Y., 2014a. J. Solid State Electrochem 19 (1), 307–314.
Wang, H., Bo, X., Guo, L., 2014b. Sens. Actuators B 192, 181–187.
Wang, H., Yuan, X., Zeng, G., Wu, Y., Liu, Y., Jiang, Q., Gu, S., 2015a. Adv. Colloid Interface Sci. 221, 41–59.
Wang, L., Wong, C.H.A., Kherzi, B., Webster, R.D., Pumera, M., 2015b. ChemCatChem 7, 1650–1654.
Wang, M., Zheng, J., 2012. J. Electrochem. Soc. 159 (6), F150–F156.
Wang, S., Yu, D., Dai, L., 2011a. J. Am. Chem. Soc. 133 (14), 5182–5185.
Wang, Y., Li, H., Kong, J., 2014c. Sens. Actuators B 193, 708–714.
Wang, Y., Shao, Y., Matson, D.W., Li, J., Lin, Y., 2010. ACS Nano 4 (4), 1790–1798.
Wang, Y., Zhang, S., Du, D., Shao, Y., Li, Z., Wang, J., Engelhard, M.H., Li, J., Lin, Y., 2011b. J. Mater. Chem. 21 (14), 5319–5325.
Wang, Z., Dai, Z., 2015. Nanoscale 7 (15), 6420–6431.
Wen, Z., Cui, S., Pu, H., Mao, S., Yu, K., Feng, X., Chen, J., 2011. Adv. Mater. 23 (45), 5445–5450.
Wong, C.H.A., Chua, C.K., Khezri, B., Webster, R.D., Pumera, M., 2013. Angew. Chem. Int. Ed. 52 (33), 8685–8688.
Wu, H., Wang, J., Kang, X., Wang, C., Wang, D., Liu, J., Aksay, I.A., Lin, Y., 2009. Talanta 80 (1), 403–406.
Wu, M., Meng, S., Wang, Q., Si, W., Huang, W., Dong, X., 2015. ACS Appl. Mater. Interfaces 7 (38), 21089–21094.
Wu, S., He, Q., Tan, C., Wang, Y., Zhang, H., 2013. Small 9 (8), 1160–1172.
Xi, F., Zhao, D., Wang, X., Chen, P., 2013. Electrochem. Commun. 26, 81–84.
Xia, X.H., Chao, D.L., Zhang, Y.Q., Shen, Z.X., Fan, H.J., 2014. Nano Today 9 (6), 785–807.
Xing, X., Liu, S., Yu, J., Lian, W., Huang, J., 2012. Biosens. Bioelectron. 31 (1), 277–283.
Xu, C., Wang, J., Wan, L., Lin, J., Wang, X., 2011a. J. Mater. Chem. 21 (28), 10463–10471.
Xu, F., Sun, Y., Zhang, Y., Shi, Y., Wen, Z., Li, Z., 2011b. Electrochem. Commun. 13 (10), 1131–1134.
Xu, G.-B., Cui, J.-M., Liu, H., Gao, G.-G., Qiu, Y.-F., Zhang, S.-M., Wu, D.-M., 2015. Electrochim. Acta 168, 32–40.
Xu, Y., Sheng, K., Li, C., Shi, G., 2010. ACS Nano 4 (7), 4324–4330.
Xue, Y., Zhao, H., Wu, Z., Li, X., He, Y., Yuan, Z., 2011. Biosens. Bioelectron. 29 (1), 102–108.
Yan, Z., Yao, W., Hu, L., Liu, D., Wang, C., Lee, C.S., 2015. Nanoscale 7 (13), 5563–5577.
Yang, C., Denno, M.E., Pyakurel, P., Venton, B.J., 2015a. Anal. Chim. Acta 887, 17–37.
Yang, G., Zhu, C., Du, D., Zhu, J., Lin, Y., 2015b. Nanoscale 7 (34), 14217–14231.
Yang, X., Li, X., Ma, X., Jia, L., Zhu, L., 2013. RSC Adv. 3 (19), 6752–6755.
Yang, X., Li, X., Ma, X., Jia, L., Zhu, L., 2014. Electroanalysis 26 (1), 139–146.
Ye, D., Liang, G., Li, H., Luo, J., Zhang, S., Chen, H., Kong, J., 2013. Talanta 116, 223–230.
Yi, M., Shen, Z., 2015. J. Mater. Chem. A 3 (22), 11700–11715.
Yi, Y., Zhu, G., Wu, X., Wang, K., 2016. Biosens. Bioelectron. 77, 353–358.
Yu, B., Kuang, D., Liu, S., Liu, C., Zhang, T., 2014a. Sens. Actuators B 205, 120–126.
Yu, D., Dai, L., 2009. J. Phys. Chem. Lett. 1 (2), 467–470.
Yu, Y., Chen, Z., He, S., Zhang, B., Li, X., Yao, M., 2014b. Biosens. Bioelectron. 52, 147–152.
Yuan, C.X., Fan, Y.R., Tao, Z., Guo, H.X., Zhang, J.X., Wang, Y.L., Shan, D.L., Lu, X.Q., 2014a. Biosens. Bioelectron. 58, 85–91.
Yuan, M., Liu, A., Zhao, M., Dong, W., Zhao, T., Wang, J., Tang, W., 2014b. Sens. Actuators B 190, 707–714.
Yuan, W., Zhou, Y., Li, Y., Li, C., Peng, H., Zhang, J., Liu, Z., Dai, L., Shi, G., 2013. Sci. Rep. 3, 2248.
Yue, H.Y., Huang, S., Chang, J., Heo, C., Yao, F., Adhikari, S., Gunes, F., Liu, L.C., Lee, T. H., Oh, E.S., Li, B., Zhang, J.J., Huy, T.Q., Luan, N.V., Lee, Y.H., 2014. ACS Nano 8 (2), 1639–1646.
Yun, S., Kang, S.-O., Park, S., Park, H.S., 2014. Nanoscale 6 (10), 5296–5302.
Zeng, Q., Cheng, J., Tang, L., Liu, X., Liu, Y., Li, J., Jiang, J., 2010. Adv. Funct. Mater. 20 (19), 3366–3372.
Zhan, B., Liu, C., Chen, H., Shi, H., Wang, L., Chen, P., Huang, W., Dong, X., 2014a. Nanoscale 6 (13), 7424–7429.
Zhan, B., Liu, C., Shi, H., Li, C., Wang, L., Huang, W., Dong, X., 2014b. Appl. Phys. Lett. 104 (24), 243704.
Zhang, B., Li, Q., Cui, T., 2012a. Biosens. Bioelectron. 31 (1), 105–109.
Zhang, H., Bo, X., Guo, L., 2015a. Sens. Actuators, B 220, 919–926.
Zhang, H., Bo, X., Guo, L., 2016. Electrochim. Acta 201, 117–124.
Zhang, H., Gai, P., Cheng, R., Wu, L., Zhang, X., Chen, J., 2013. Anal. Methods 5 (14), 3591.
Zhang, L., Han, G., Liu, Y., Tang, J., Tang, W., 2014. Sens. Actuators, B 197, 164–171.
Zhang, S., Shao, Y., Liao, H.-G., Liu, J., Aksay, I.A., Yin, G., Lin, Y., 2011a. Chem. Mater. 23 (5), 1079–1081.
Zhang, W., Chai, Y., Yuan, R., Chen, S., Han, J., Yuan, D., 2012b. Anal. Chim. Acta 756, 7–12.
Zhang, X., Li, S., Jin, X., Zhang, S., 2011b. Chem. Commun. 47 (17), 4929–4931.
Zhang, Y., Xu, F., Sun, Y., Shi, Y., Wen, Z., Li, Z., 2011c. J. Mater. Chem. 21 (42), 16949–16954.
Zhang, Z., Cai, R., Long, F., Wang, J., 2015b. Talanta 134, 435–442.
Zhao, Y., Bo, X., Guo, L., 2015. Electrochim. Acta 176, 1272–1279.
Zhou, J., Chen, M., Diao, G., 2013. ACS Appl. Mater. Interfaces 5 (3), 828–836.
Zhou, K., Zhu, Y., Yang, X., Luo, J., Li, C., Luan, S., 2010. Electrochim. Acta 55 (9), 3055–3060.
Zhou, M., Guo, S., 2015. ChemCatChem 7 (18), 2744–2764.
Zhou, M., Zhai, Y., Dong, S., 2009. Anal. Chem. 81 (14), 5603–5613.
Zhu, C., Guo, S., Zhai, Y., Dong, S., 2010. Langmuir 26 (10), 7614–7618.
Zhu, G., Yi, Y., Zou, B., Liu, Z., Sun, J., Wu, X., 2014. Microchim. Acta 182 (3–4), 871–877.
Zhu, L., Luo, L., Wang, Z., 2012. Biosens. Bioelectron. 35 (1), 507–511.
Zhu, Y., Murali, S., Stoller, M.D., Ganesh, K., Cai, W., Ferreira, P.J., Pirkle, A., Wallace, R.M., Cychosz, K.A., Thommes, M., 2011. Science 332 (6037), 1537–1541.